METHYL MERCURY HOTSPOTS AND SOURCES IN THE GREAT SALT LAKE, UTAH, ADJACENT FRESHWATER BAYS AND IMPOUNDED WETLANDS

by

Brooks M. Black and Neil P. Swanson

A thesis submitted to the faculty of
The University of Utah
in partial fulfillment of the requirements for the degree of

Master of Science

in

Geological Engineering

Department of Geology and Geophysics

The University of Utah

December 2013

THE UNIVERSITY OF UTAH GRADUATE SCHOOL

STATEMENT OF THESIS APPROVAL

The thesis of **Brooks M. Black**

has been approved by the following supervisory committee members:

William P. Johnson	, Chair	**5-7-2013** Date Approved
Diego P. Fernandez	, Member	**5-7-2013** Date Approved
John R. Bowman	, Member	**5-7-2013** Date Approved

and by **John M. Bartley** , Chair of

the Department of **Geology and Geophysics**

and by David B. Kieda, Dean of The Graduate School.

ABSTRACT

Water column, sediment and pore water samples were collected from multiple locations of the Great Salt Lake (GSL), Utah to examine the spatial and temporal distribution of total mercury (THg) and methyl mercury (MeHg) concentrations and MeHg production potentials (MPPs). Sampling locations included multiple transects in the south arm of the GSL, adjacent freshwater influenced bays, and multiple impounded and sheet flow freshwater wetland sites during the period of summer 2009-summer 2012. Select water column and sediment subsamples were spiked with inorganic mercury ($I^{204}Hg$) and methyl mercury ($Me^{204}Hg$) to examine net production of methyl mercury ($Me^{204}Hg$) and net loss of $Me^{201}Hg$. First order methylation (k_{meth}) and demethylation (k_{demeth}) rate constants were determined from changes in isotope dilution corrected concentrations and/or changes in isotope ratios as a function of time. Tin reducible inorganic Hg ($Hg(II)_R$) was used as a proxy for bioavailable Hg(II) in GSL samples. MeHg production potentials (MPPs) were calculated as the time integrated product of k_{meth} and $Hg(II)_R$ to compare methylation in deep brine layer (DBL) versus underlying sediment slurry (SSL) samples of the GSL. A large range of methylation rate constants (1.4E-6 to 1.1E-3 hr^{-1}) was observed across the region, whereas demethylation was only significant in the DBL. Positive correlation of k_{meth} to organic matter content was observed in sediment of the freshwater influenced bays and impounded wetlands, while this trend was not observed in DBL and SSL of the GSL. These results further indicate

that sediment organic matter, as well as other factors (e.g., organic matter lability and sulfide concentrations) contribute to production of MeHg. Spatially, higher MeHg concentrations in the GSL and sheet flow freshwater wetlands present the possibility of 'hot spots' for MeHg introduction into the food web. Greater and temporally constant MPPs in SSL relative to DBL may explain the persistence of high MeHg concentrations in the DBL.

TABLE OF CONTENTS

LIST OF FIGURES

LIST OF TABLES

ACKNOWLEDGMENTS

This research was supported by funding from the Division of Forestry, Fire, and State Lands (FFSL) of the Utah Department of Natural Resources, Jordan River/Farmington Bay Water Quality Council, and Central Davis Sewer District. Additionally, we would like to thank Michelle Arias (USGS, Menlo Park) for $Hg(II)_R$ assays.

CHAPTER 1

INTRODUCTION

The Great Salt Lake (GSL), located in northwestern Utah, is the largest terminal lake in the western hemisphere, and is an important ecosystem for a migratory bird population in the millions. Due to the over 1.4 million shorebirds using the GSL and surrounding wetlands for breeding and staging areas the Western Hemisphere Shorebird Reserve Network has recognized the GSL as a site of hemispheric importance (Aldrich and Paul, 2002). Consumption advisories have been issued by the Utah Department of Health for three species of waterfowl found in the GSL system due to duck muscle tissue total mercury (Hg) levels that exceed the EPA screening value (0.3 $mg\text{-}kg^{-1}$) (Scholl and Ball, 2006). Elevated Hg concentrations have also been found in California gulls and Eared grebes nesting on the GSL (Conover and Vest, 2009a, 2009b).

At approximately the same time that high Hg concentrations were recognized in some waterfowl on the GSL in 2007, exceptionally high methyl mercury (MeHg) concentrations were found in the deep brine layer (DBL) of the GSL (Naftz et al., 2008), ranging from 0.8 to >30 $ng\text{-}L^{-1}$. The DBL arises from a strong salinity contrast between the north and south arms of the GSL, which are separated by a railroad causeway. Higher salinity water flows from the north to the south arm through breaches in the causeway (and the permeable fill material), and pools in the south arm, and is not subject to annual

turnover because of the salinity difference (Naftz et al., 2008; Gwynn, 2002; Loving et al., 2002). Since MeHg is the bioaccumulative form of Hg (Baeyens et al., 2003; Mason et al., 2006), these high MeHg concentrations in the DBL indicate a possible connection to elevated MeHg in waterfowl. Whereas the thickness of the DBL varies seasonally and annually, its primary characteristics include: a) anoxia (Gwynn, 2002; Diaz et al., 2009); b) high dissolved sulfide concentrations (up to several tens of mg-L^{-1}) (Naftz et al., 2008); c) high organic carbon content ranging from ~60-90 mg-L^{-1} (Diaz et al., 2009; Supporting Information), all of which have been associated with MeHg production (Graham et al., 2012; Sunderland et al., 2006; King et al., 2000).

Entry of MeHg into the ecosystem may not be related to the DBL, but rather may occur within the freshwater wetlands on the eastern boundary of the GSL. Diurnal nighttime MeHg production has been documented in a particular impounded wetland pond (Naftz et al., 2011). However, ponds nearby the one that produced MeHg during nighttime hours showed no such MeHg production (Carling et al., 2011). These results suggest significant spatial variability in MeHg concentrations and MeHg production among the impounded wetland ponds, and suggest the possible presence of MeHg "hotspots" wherein linkage to biota may occur.

This study investigates the spatial and temporal distribution of total mercury (THg) and MeHg concentrations and MeHg production potential across the GSL, spanning the main (south) arm of the GSL, freshwater influenced bays, and impounded and sheet flow freshwater wetlands during the period summer 2009-summer 2012. Concentrations and MeHg production potentials were determined in multiple media (water column, sediment and pore water) across these settings in order to identify

locations and media with relatively elevated THg and MeHg concentrations and greater MeHg production potentials.

CHAPTER 2

METHODS

2.1 Locations

Three geographic locations were examined: South arm (main body) of the GSL, freshwater influenced bays (Ogden and Farmington Bays), freshwater impounded wetlands (16 locations) and sheet flow wetlands (5 sites) adjacent to the freshwater influenced bays (Figure 1).

2.2 Media

Three types of media were collected from these locations: water column, sediment and pore water, with the exception that water column samples were not collected in the sheet flow wetlands (negligible water column depth) and pore water was not collected in the freshwater-influenced bays. The target water column in the GSL was the DBL, and the target sediment in the GSL was the fine, unconsolidated, organic rich sediment slurry (SSL) underlying the DBL.

2.3 Frequency

Samples were collected during the period from summer 2009 to summer 2012. In the south arm of the GSL, 3 transects were sampled in August 2011 (3 sites each), April and July 2012 (2 sites each). In freshwater influenced Ogden and Farmington Bays (OB and

FB, respectively), two 5-site FB transects were sampled in late July (referred to as summer) and October (referred to as fall), 2009, and one 5-site OB transect was sampledin August, 2010. In the freshwater impounded wetlands, 16 locations were sampled throughout summer (June-September) 2012 and 5 corresponding locations throughout summer 2010-2011, with varying frequency of two to four times each summer. In the sheet flow wetlands, 5 locations were sampled during June and July 2011.

2.4 Sample collection

Water column samples were collected by two different methods: a) peristaltic pump (GSL and bays); b) bottles by hand (wetlands). Samples were stored on ice in the field, transferred to a refrigerator in the laboratory, and analyzed within one week (anions, DOC, "reactive" inorganic mercury ($Hg(II)_R$)), or three months (total mercury (THg)/MeHg, trace/major elements) of collection. Collection by peristaltic pump was performed with acid-washed PTFE tubing. "Clean hands/dirty hands" protocol (USEPA, 1996) was used for THg/MeHg collection. Anoxic samples were filled to overflowing while headspace was N_2 purged, tightly capped and taped (electrical) to prevent exposure to air. Storage bottles, corresponding analytes and sample preservatives used arprovided in Table 1. Select analytes were also filtered inline using a cartridge filter (0.45 μm, Geotech). Collection by hand was performed for oxic waters only using a 60-mL polyethylene syringe with a 0.45-μm PES filter (Whatman International Ltd.). Filters were precleaned by flushing with 10% $v\text{-}v^{-1}$ TMG HCl (50 mL) followed by three 50-mL rinses (Milli-Q). Storage bottles, corresponding analytes and sample preservatives used were the same as for anoxic samples (Table 1).

Sediment slurry (SSL) and sediment samples were collected by two different methods: a) peristaltic pump (SSL of the GSL); b) anoxic cores (bays and wetlands). Samples were stored on ice in the field, transferred to a freezer in the laboratory, and run within six months of collection. SSL samples collected by peristaltic pump were stored in 500 mL triple-rinsed FLPE bottles, filled to overflowing while headspace was N_2 purged, tightly capped and taped (electrical) to prevent exposure to air. Anoxic cores were collected using cellulose acetate butyrate tubing (CAB) inserted vertically into sediment. The exposed end was capped and sealed with electrical tape to create a vacuum. The bottom of tube was capped under water and sealed with electrical tape. Top end of the tube was cut and overlying water was drained to 5-6 cm above the sediment surface and recapped and taped to preserve anoxia.

Pore water samples were collected using acrylic core squeezers as described below. Bottles, analytes and preservation methods are described in Table 1. Because pore water was anoxic and sample volume was limited bottles were filled to minimize head space (not overflowing). Core squeezers contained predrilled ports for pore water sampling. Five cm length Porex rods (30-70 μm pore size) connected to 0.45 μm PES syringe filters by a Leur adapter were inserted through sample ports. Pore water was collected, out of sunlight, using a 30 mL polyethylene syringe connected to syringe filter after several drops passed to prevent collection of oxidized water by applying pressure using pistons inserted on both ends of acrylic tube as described in Chin et al. (1998)

Field measurements included dissolved oxygen (DO), temperature (T), conductivity, and pH, all measured in the water column using a field probe (YSI Professional Series Quatro). Sulfide was measured in filtered water column and pore

water samples immediately after collection (V-2000 Multi-analyte LED Photometer and Vacu-vials®, CHEMetrix).

2.5 Sample preparation

Methylation and demethylation rates were determined in select samples spiked with inorganic ($I^{204}Hg$), and methyl ($Me\ ^{201}Hg$) mercury, respectively. These samples were prepared under argon in a glove box (Vacuum Glovebox VGB, MTI Corporation), within 12 hours of sample collection. Tracer spikes were obtained from Oak Ridge National Laboratory (Oak Ridge, TN) as Hg (II) oxide (98.11% purity) for $I^{204}Hg$ and from Applied Isotope Technologies, Inc. as C_2H_5HgCl (98.11% purity) for $Me^{201}Hg$. Isotope tracer concentrations were targeted to match initial THg and MeHg concentrations (total of all isotopes). However, not all ambient THg and MeHg concentrations were known *a priori*, in which case estimates were made based on closest existing data. $I^{204}Hg$ and $Me^{201}Hg$ tracer spike concentrations were within a factor of three of ambient concentrations for 74% and 65% of samples, respectively, and a factor of 10 for 97% ($I^{204}Hg$) and 85% ($Me^{201}Hg$) of isotope tracer spikes, respectively. A complete table of isotope tracer spike concentrations (represented as % ambient concentrations) is in the Supporting Information. Spikes were added via pipette to sample aliquots (200 g water column, 50 g sediment), which were homogenized by stirring to obtain the desired concentrations.

Following spike addition, samples were subsectioned to allow multiple incubation times in parallel subsamples. Subsamples were placed into crimp-top serum bottles with chlorobutyl-isoprene blend septa, 50 mL (water column), and 10 mL (sediment and SSL), with replicates for analysis pre- and postspiking for isotope dilution correction (described

below). Subsample incubation was performed at room temperature on a shaker table (130 rpm). Incubation was quenched via addition of TMG HCl (1% v-v^{-1}) and refrigeration (water column samples), or flash freezing (ethanol bath in -20°C freezer) (sediment and SSL samples).

Sample preparation for THg, MeHg, and $Hg(II)_R$ analyses depended on the sample medium. Water column and pore water samples were acidified with trace metal grade (TMG) HCl to 1% after collection and oxidized in-bottle via BrCl (24 hours) prior to THg analyses, and were distilled with ammonium pyrrolidine dithiocarbamate (APDC) prior to MeHg analyses. Water column samples (DBL) were prepared for $Hg(II)_R$ analysis as described in Marvin-DiPasquale and Cox, 2007. Sediment samples were prepared for THg analysis, as described below, by digestion (1 g in 5 mL 7:3 TMG HNO_3/H_2SO_4 at 80^{o}C for 6 hours), followed by dilution in BrCl solution (5%), following EPA Method 1631-appendix (USEPA, 2001b). Sediment samples were prepared for MeHg analysis by extraction, as described in Bloom et al. (1997). One gram of sediment reacted with 5 mL of KBr/H_2SO_4 solution (18% w-v^{-1} KBr, 5% v-v^{-1} TMG H_2SO_4) and 1 mL $CuSO_4$ (1 M). MeHg was extracted from the solution using methylene chloride (10 mL), of which 2 mL were pipetted into a Teflon distillation tube, and then submerged in 50 mL of MilliQ water. Following complete evaporation of methylene chloride (1-2 hours at 55°C, purged with ultra-high purity N_2), the pure MeHg in water was analyzed as described below. Sediment samples were prepared for $Hg(II)_R$ analysis as described in Marvin-DiPasquale and Cox, 2007.

For GSL methylation/demethylation subsamples, an isotope dilution (ID) spike, $Me^{200}Hg$ (Applied Isotope Technologies, Inc. as CH_3HgCl, 96.17% purity) was added

prior to distillation (water column samples) or extraction (SSL samples) via glass syringe through chlorobutyl-isoprene blend septa. ID spike concentrations were matched to ambient when known, and otherwise were based on closest existing data. ID spike concentrations were within factors of three and 10 of ambient MeHg concentrations for 75% and 95% of samples, respectively (Supporting Information).

Sediment samples were prepared for trace element and major cation analyses by leaching sediment (1 g in 20 mL 5% $v\text{-}v^{-1}$ TMG HCl) at room temperature for three days, followed by centrifugation and analysis of supernatant using ICP-MS (as described below). This was not a complete digestion; rather, a weak acid leach intended to recover the bioavailable trace element fraction.

Prior to organic carbon analyses (described below), SSL samples were oven-dried at 105 ^{o}C, and were then ground to a fineness of roughly 0.01 mm using a stainless steel ball mill (Mixer Mill MM 200, Retsch GmbH) in a 25 mL container at 30 RPS for one minute. Inorganic carbon was digested using 0.5 M HCl until the acidified SSL solution maintained a pH of 1 or less, and the digestive sample was filtered from solution through 7 cm diameter hardened glass filter paper (Whatman International Ltd.), and then oven dried prior to analysis.

2.6 Sample analysis

THg, MeHg, and $Hg(II)_R$ analysis was performed using cold vapor adsorption atomic fluorescence spectroscopy (CVAFS) (Model III, Brooks Rand Labs, LLC). THg and MeHg analyses were performed using EPA Methods 1631e (USEPA, 2002) and 1630 (USEPA, 2001a), respectively. $Hg(II)_R$ analysis ($SnCl_2$ reducible Hg(II)) was performed as previously described (Marvin-DiPasquale and Cox, 2007).

To assess the quality of data, matrix spike recoveries, certified reference materials (CRM) and isotope dilution were used. Interlaboratory comparisons were used to assess accuracy of our laboratory. For water column, pore water, and sediment samples, recovery was quantified using matrix spikes and isotope dilution, the latter for DBL and SSL samples only (as described further below). THg and MeHg matrix spike recoveries were analyzed for every 10 samples, with recoveries for acceptance being 70-130% for all phases (THg and MeHg water column and pore water, THg sediment/SSL). MeHg recoveries in impounded wetland sediment samples ranged 50-93%, with an average recovery of 67% ± 16% (n=6). CRMs were used as a proxy for both THg and MeHg recoveries from SSL and sediment samples. CRMs were analyzed at a minimum every 10 samples. For THg the CRM used was MESS-3 (Canadian National Research Council, Ottawa, Ontario, Canada) marine sediment. THg recovery from the CRM was 103% ± 15%. (n=17). The MeHg CRM used was CC580 estuarine marine sediment (European Reference Materials Institute for Reference Materials and Measurements, Geel, Belgium). MeHg recovery was 74% ± 21% (n=30). Interlaboratory comparison tests in 2011 and 2012 for THg and MeHg in water column samples (40 laboratories, round robin, conducted by Brooks Rand Labs, LLC) showed that results from our laboratory fell within ± 20% of the mean reported value.

Dissolved organic carbon (DOC) was measured in water column and pore water samples (TOC-5000a, Shimadzu, Inc.) within one week of sample collection. Sediment dry weight and Total Volatile Solids (TVS), calculated as % loss on ignition (LOI), were measured in wetland and freshwater bay sediment following drying (24 hours at 105°C), ignition at 500°C (2 hours), according to EPA Method 1684 (USEPA, 2001c). Percent

organic carbon was measured using a Delta Plus isotope ratio mass spectrometer (Finnifan-MAT, Bremen Germany) interfaced with an Elemental Analyzer (model 1110, Carla Erba, Milan, Italy) for SSL samples.

Trace and major elements were measured using a quadrupole ICP-MS (Agilent 7500ce, Agilent Technologies) with a collision cell, a double-pass spray chamber with perfluoroalkoxy fluorocarbon (PFA) nebulizer (0.1 mL-minute^{-1}), a quartz torch, and platinum cones. Samples were analyzed within six months of collection, which is an acceptable holding time for trace elements (USEPA, 1994). Concentrations were measured for the following elements: Ag, Al, As, Ba, Be, Ca, Cd, Co, Cr, Cu, Fe, K, Li, Mg, Mn, Mo, Na, Ni, Pb, Sb, Se, Sr, Ti, Tl, U, V and Zn. In 2012, Cs, P, Rb, Tl, and a selection of rare earth elements were additionally analyzed. Further details are provided in Carling et al. (2013). Major anion concentrations were measured using ion chromatography (IC) within 2 weeks of sample collection, as described in Carling et al. (2013).

2.7 Data analysis

Isotope dilution (ID) (Hintelmann and Evans, 1997) was used to correct for extraction inefficiencies in determining isotope concentrations, based on recovery of the ID isotope ($Me^{200}Hg$) as follows:

$$C_{204}^{preID} = \frac{m_{204}^{Me200ID}\left(R_{\frac{200}{204}}^{Me200ID} - R_{\frac{200}{204}}^{postID}\right)}{sample\ mass\left(R_{\frac{200}{204}}^{postID} - R_{\frac{200}{204}}^{preID}\right)} \quad [1]$$

where, $C^{preID}{}_{204}$ is the ID-corrected concentration of $Me^{204}Hg$, $m^{Me200ID}{}_{204}$ is the mass of $Me^{204}Hg$ in the enriched $Me^{200}Hg$ ID spike, $R^{Me200ID}{}_{200/204}$ is the ratio of $Me^{200}Hg$ to $Me^{204}Hg$ in the ID spike, $R^{postID}{}_{200/204}$ is the ratio of $Me^{200}Hg$ to $Me^{204}Hg$ in the sample

post-ID spike addition, $R^{preID}_{200/204}$ is the ratio of $Me^{200}Hg$ to $Me^{204}Hg$ in the sample pre-ID spike addition and *sample mass* corresponds to that which the ID spike is added.

Finite difference was used to back-out methylation and demethylation rate constants (k_{meth} and k_{demeth}, respectively) from either the ID-corrected concentrations (GSL samples) or isotope count ratios (GSL, bay, and wetland samples). k_{meth} and k_{demeth} were determined from ID-corrected concentrations according to the equations below (Marvin-DiPasquale et al., 2008):

$$k_{meth} = ln[1 - f_m]/t \quad [2]$$

$$k_{demeth} = ln[1 - f_d]/t \quad [3]$$

where f_m is the fraction of $[I^{204}Hg]$ converted to $[Me^{204}Hg]$, f_d is the fraction of $[Me^{201}Hg]$ converted to $[I^{201}Hg]$ (brackets here refer to concentrations), and t is the time of incubation. k_{meth} was also determined from isotope count ratios using a spreadsheet to numerically approximate the methylation/demethylation process according to the equation below:

$$[Me^{204}Hg]_t = [Me^{204}Hg]_{t-1} + k_{meth}[i^{204}Hg]_{t-1}\Delta t - k_{demeth}[Me^{204}Hg]_{t-1}\Delta t \quad [4]$$

where the time series was simulated for all measured MeHg isotopes (200, 201, 202, 204), t and $t-1$ represent present and previous time steps, respectively, and Δt is the length of the time step. Because the conditions influencing k_{meth} and k_{demeth} in the serum vials likely evolved over the course of incubation, the concentrations corresponding to the first two sample times were emphasized to determine k_{meth} and k_{demeth}.

2.8 Division of labor

Impounded and sheet flow wetlands methylation potentials and concentrations were conducted by Greg Carling. Freshwater influenced bays methylation potentials and concentrations were conducted by Abigail Rudd. GSL SSL methylation potentials and concentrations were collected by Brooks Black. GSL DBL methylation potentials and concentrations were collected by Neil Swanson.

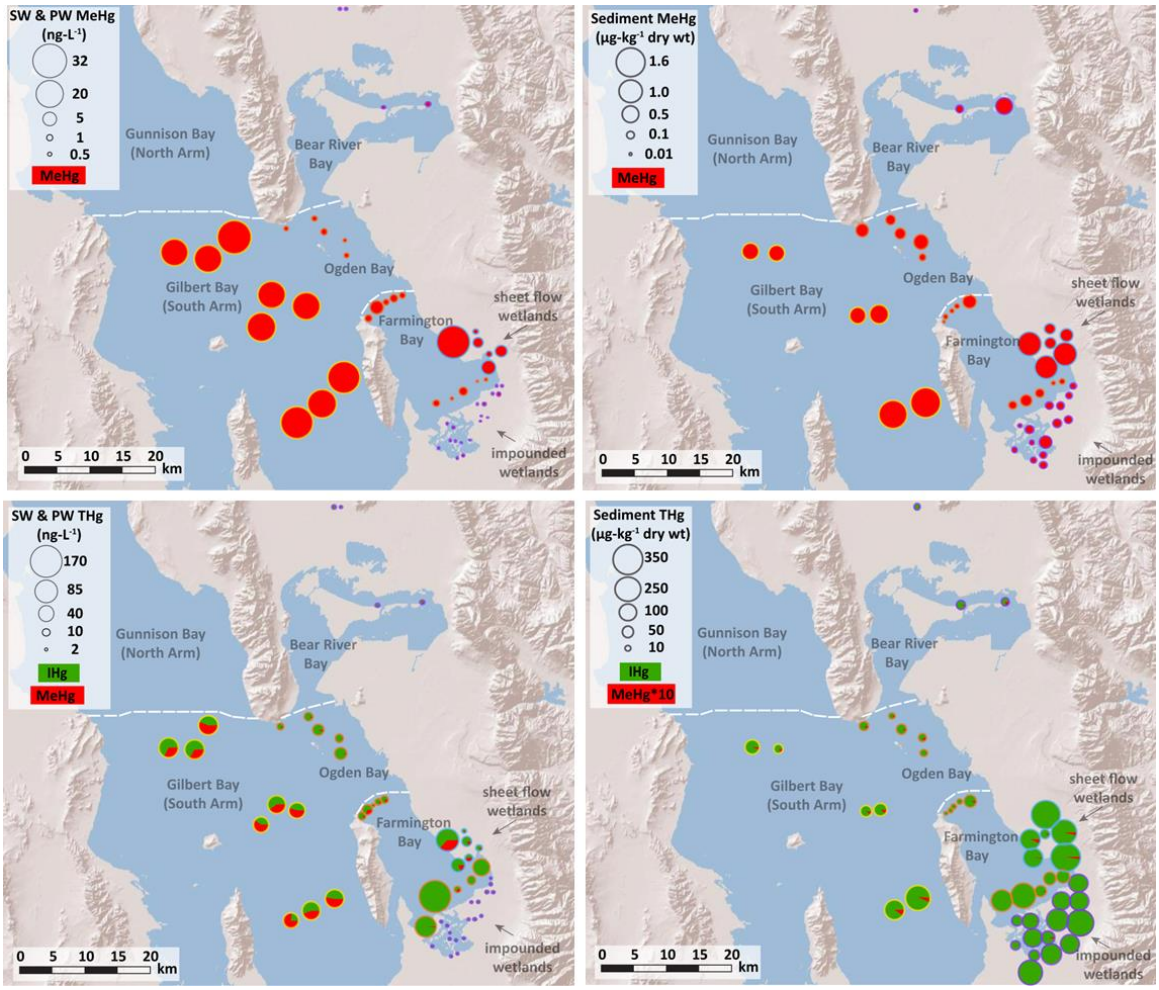

Figure 1. Maps of the Great Salt Lake (Utah) showing locations of sampling sites and corresponding mercury concentrations. Circle outline color corresponds to sampling location as follows: yellow for south arm of the Great Salt Lake, orange for freshwater influenced bays, blue for sheet flow wetlands, and purple for impounded wetlands. Top panels: circle size corresponds to MeHg concentrations (shown in red). Small symbols in impounded wetlands appear purple due to outline. Concentrations were averaged across replicate samples and time series where available. Bottom panels: circle size corresponds to total mercury (Hg) concentrations, inorganic mercury (IHg) (shown in green) was calculated via difference between Hg and methyl mercury (MeHg) (shown in red). Left panels represent water column and pore water samples. Right panels represent SSL and sediment samples. Among water column samples, DBL and freshwater influenced bay samples were unfiltered. All impounded wetland samples were filtered. SSL and sediment %MeHg concentrations (bottom right panel) were multiplied by a factor of 10 to make visible the small fractions of Hg comprised by MeHg in these samples. Exact locations and concentrations with standard deviations are given in Supporting Information.

Table 1. Water column and pore water analytes, storage bottle preparation, and corresponding sample preservation.

	THg/MeHg	Major/Trace Elements	Major Anions	Dissolved Organic Carbon
Storage Bottles	250 mL FLPE	30 mL LDPE	30 mL LDPE	30 mL amber glass
Storage Bottle Preparation	Triple rinse (Milli-Q)	10% v/v HCl leach at 60 °C (48 hours) followed by triple rinse (Milli-Q)	Triple rinse	10% v/v HCl leach at 60 °C (24 hours) followed by triple rinse (Milli-Q)
Sample Preservation	1% v/v TMG HCl	2.4% v/v TMG HNO_3	No head space	No head space

CHAPTER 3

RESULTS

3.1 Mercury concentrations

Mercury concentrations for each location and each phase were averaged across replicate samples and time series where available (Figure 1). Spatially, the highest averaged MeHg concentrations in surface water and pore water samples were measured in the water column and pore water of the south arm of the GSL (deep brine layer) and sheet flow wetlands, respectively. Similarly, the highest averaged MeHg concentrations in sediment samples were measured in the south arm of the Great Salt Lake (sediment slurry underlying the deep brine layer) and sheet flow wetlands. Although the high MeHg concentrations in the DBL are spatially invariable, the high MeHg concentrations in the SSL are spatially variable, with the highest averaged concentrations measured in the southern portion of the south arm of GSL. Furthermore, water column and pore water samples have higher measured fractional MeHg (%MeHg/THg) concentrations than in sediment samples; however, it is important to note that MeHg concentrations in sediment samples are on average more than 100 times greater than in water samples. The spatial variation in averaged MeHg concentrations and fractional MeHg concentrations for all sampling settings and media are listed below. Tabular values for concentrations and standard deviations are provided in Supporting Information.

Comparing across all sites for the water column, sediment and pore water phases

(Figure 1), the highest MeHg concentrations occur in the DBL and SSL of the GSL and the pore water and sediment of the sheet flow wetlands. MeHg concentration ranges in water column and pore water samples from highest to lowest were: 21-32 ng-L^{-1} (DBL), 0.7-30.7 ng-L^{-1} (sheet flow pore water), 0.1-4.9 ng-L^{-1} (freshwater influenced bay water column), 0.03-0.48 ng-L^{-1} (impounded wetland water column), 0.07-0.10 ng-L^{-1} (impounded wetland pore water). MeHg concentration ranges in SSL and sediment samples from highest to lowest were: 440-1600 ng-kg^{-1} dw (SSL), and 190-980 ng-kg^{-1} dw (sheet flow sediment), 20-500 ng-kg^{-1} dw (impounded wetland sediment), and 20-410 ng-kg^{-1} dw (freshwater influenced bays).

Fractional MeHg (MeHg/THg) concentration ranges in water column and pore water samples from highest to lowest were: 37-60% (DBL), 17-43% (sheet flow pore water), 0.1-29.6% (freshwater influenced bay water column), 3-28% (impounded wetland water column), 4-7% (impounded wetland pore water). The high fractional MeHg concentrations in the DBL are more impressive by the fact that these samples were unfiltered. Fractional MeHg (MeHg/THg) concentration ranges in SSL and sediment samples from highest to lowest were: 0.56-1.44% (SSL), 0.09-0.54% (sheet flow sediment), 0.03-2.16% (impounded wetland sediment), and 0.03-1.65% (freshwater influenced bays).

Water column MeHg concentrations showed no clear temporal trend. In contrast, SSL and sediment MeHg concentrations showed a clear decreasing trend across the warm season in 2012, when sampling spanned a larger period (April-September, as opposed to August-September in previous years). This is shown in Figure 2, where bars correspond to absolute decreases of MeHg concentrations from first and last months sampled.

Despite different early season and late season dates across the sites, the general trend of higher MeHg concentrations in early season relative to late season is apparent, with only one site showing a significant increase, and the majority of sites showing a decrease, in MeHg concentration (up to several hundred ng-kg^{-1}).

3.2 Methylation

Methylation, as measured by MeHg concentration changes (and/or $Me^{202}Hg$/ $Me^{204}Hg$ ratio changes) in spiked samples during incubation, were negligible in water column samples except DBL, significant in nearly all SSL and sediment samples, greater in SSL versus DBL, and were greater in April versus July (SSL and DBL) (Figure 3). While the greater MeHg production in SSL relative to DBL in incubated samples is obvious, the IHg reservoir that may potentially be methylated was a hundred to a thousand times greater in SSL relative to DBL. On this basis alone, one might expect greater MeHg production in SSL relative to DBL. Methylation (and demethylation) rate constants attempt to account for this IHg reservoir.

Table 2 shows the range of methylation and demethylation rate constants according to location. The full set of rate constants are provided in the Supporting Information. A large range (factor of 1,000) of k_{meth} values (1.4E-6 to 1.1E-3 hr^{-1}) was observed across the region. This entire range was observed in the Farmington Bay North location; however, the range at the other locations fell mostly within an order of magnitude, except DBL, which ranged over a factor of 30. This spatial variation within the DBL did not correspond to variation in (for example) DOC, trace elements, SO_4^{2-}, or dissolved S^{2-}, all of which showed little spatial variation in the DBL (Supporting Information).

Values of k_{meth} from the DBL bracketed those from the SSL (overall range from 1.1 E-3 to 2.1 E-5 hr^{-1}) despite the vast differences in measured MeHg concentration changes between those two media during incubation (Figure 3). Values of k_{meth} showed an average decrease of 64% (SSL) and nearly two orders of magnitude (DBL) from April to July (Supporting Information), suggesting an overall decrease in methylation in the GSL system over the course of the summer.

Whereas modest methylation was observed in the DBL, robust demethylation was characteristic of the DBL, with rate constants ranging from 3.0E-2 to 1.8E-1 hr^{-1}. In contrast, minimal demethylation was observed in SSL samples. Demethylation was observed at only one SSL site in April (C1 at 2.7 E-2 hr^{-1}) and only one SSL site in July (B1 at 1.9 E-2 hr^{-1}).

Rate constants (k_{meth} and k_{demeth}) for DBL and SSL samples were obtained using both ID-corrected concentrations and isotope ratios. In contrast, methylation rate constants for freshwater influenced bays and impounded wetlands were obtained solely using isotope ratios. Figure 4 displays the equivalence of rate constants determined using ID-corrected concentrations (left) and isotope ratios (right) for a representative site (SSL site A1 from April 2012). A single rate constant was able to fit trends in both ID-corrected concentrations and isotope ratios effectively. These fits are shown for all sites (DBL and SSL) in the Supporting Information. Overall the discrepancy between ID-corrected- and isotope ratio-based k_{meth} values (measured as the absolute value of the difference normalized to the ID-corrected k_{meth} value) was small. The maximum and average discrepancies were 84% and 39% (SSL), and 24% and 11% (DBL). These

discrepancies are small relative to the factors of 10 and 30 variation, respectively, in the SSL and DBL k_{meth} values.

Comparison of k_{meth} values across multiple phases (SSL, sediment, DBL) and different locations (Table 2) is difficult because while rate constants provide a measure of methylation and demethylation, they are imperfect, as many processes are inherently lumped into the constant. In particular, the IHg reservoir may not be fully bioavailable. The fraction of IHg that is bioavailable is governed by many complex processes, including S^{2-}concentration, microbial community structure, natural organic matter (NOM) concentration, and the size range of particle-associated mercury (Hsu-Kim et al., 2013; Gerbig et al., 2011; Zhang et al., 2012). Typically the IHg spike is expected to be more labile than the ambient IHg (Hintelmann et al., 2000), and this expectation would be reflected in experiments by negligible change in ambient (nonspiked) isotope concentrations/ratios. Because this expectation was met in DBL subsamples (Figure 5), only the spike was considered labile in DBL subsamples. In Figure 5, a representative result shows that ambient isotopes $Me^{200}Hg$ and $Me^{202}Hg$ each maintained constant values despite robust demethylation of spiked $Me^{201}Hg$. Considering both spike and ambient MeHg to be labile produces an erroneous simulated decrease in ambient isotope MeHg concentrations (Figure 5, right). Because the above expectation was not met in SSL and sediment subsamples (Figure 4, left), both ambient and spiked Hg were considered labile in these subsamples. In Figure 4 left, a representative result shows that ambient isotopes each responded similarly to $Me^{204}Hg$; whereas, in results with low methylation, these ambient isotopes more closely tracked spiked $Me^{201}Hg$ (see Supporting Information).

The labile fraction of IHg can be represented by "reactive"' inorganic mercury ($Hg(II)_R$) (Marvin-DiPasquale et al., 2008) to develop MeHg production potentials (MPP). $Hg(II)_R$ concentrations were measured at select GSL sites to produce MPP rates (Figure 6) (units = ng-kg^{-1} -hr^{-1}), as calculated according to the equation below:

$$MPP = [Hg(II)_R - Hg(II)_R \cdot exp(-k_{meth} \cdot t)]/t \quad [5]$$

where *t* is time (hours), and $Hg(II)_R$ refers to SSL wet weight concentrations and DBL mass concentrations. Based on MPPs, the SSL is a much greater source of MeHg relative to the DBL (Figure 6).

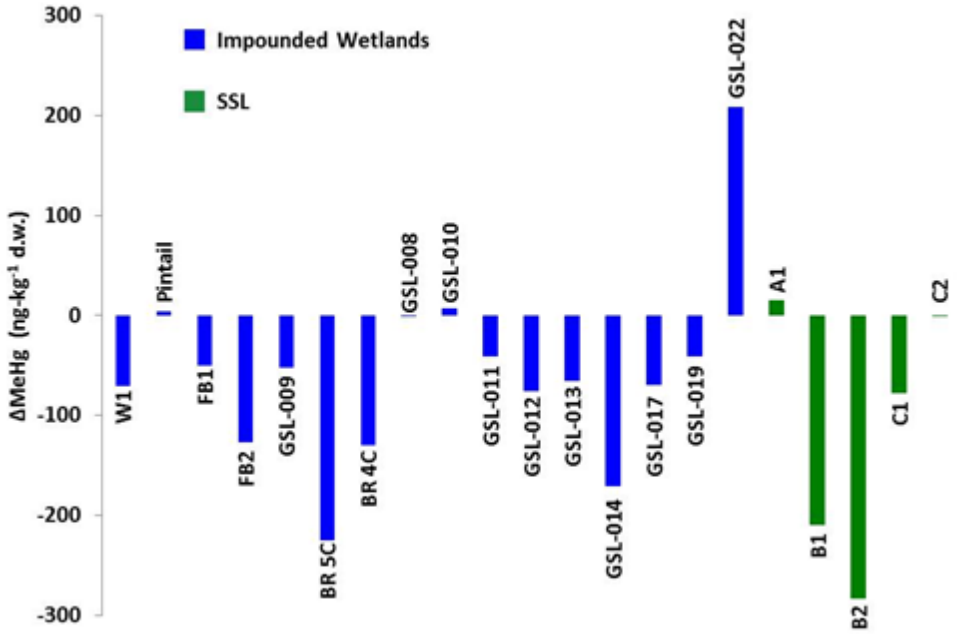

Figure 2. Sediment and SSL MeHg concentration changes (ng-kg^{-1} d.w.) from first and last months sampled in from freshwater impounded wetlands (June-September 2012) and south arm of GSL (April-July 2012). Site specific concentrations provided in Supporting Information.

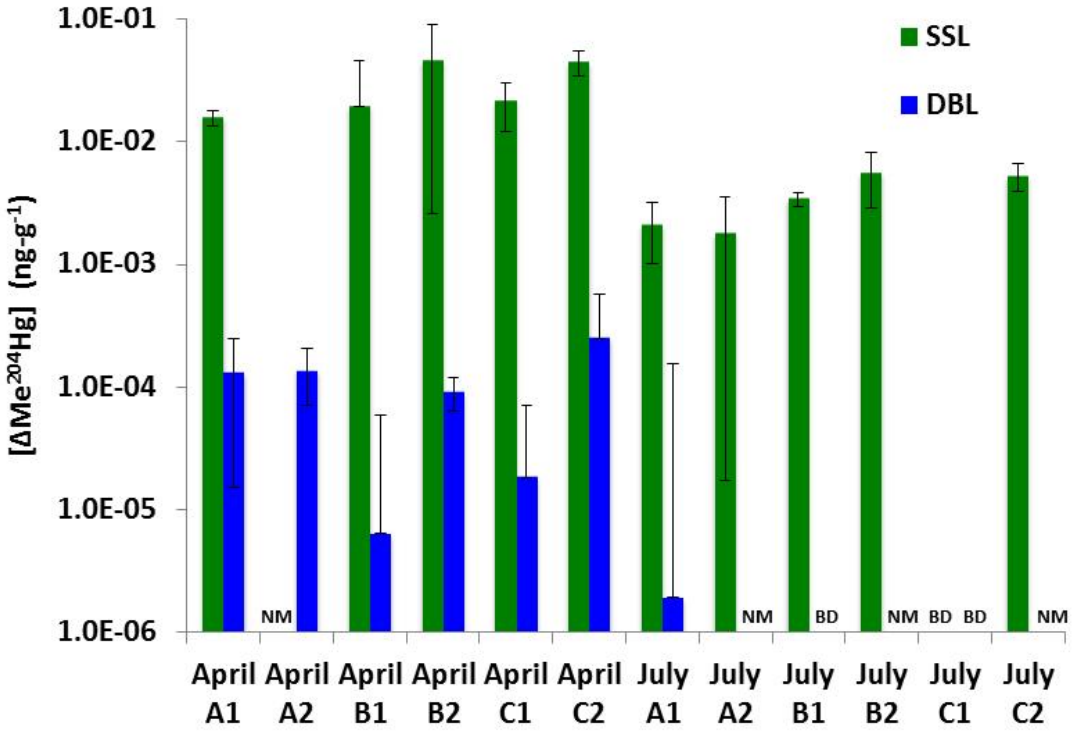

Figure 3. SSL (left) and DBL (right) ID-corrected $Me^{204}Hg$ concentration (wet weight in SSL) changes between time of spike and 2 hours for April and July 2012. The vertical axis for the DBL is two orders of magnitude smaller than that of the SSL. Error bars indicate uncertainty in the $Me^{204}Hg$ concentration changes, calculated by error propagation.

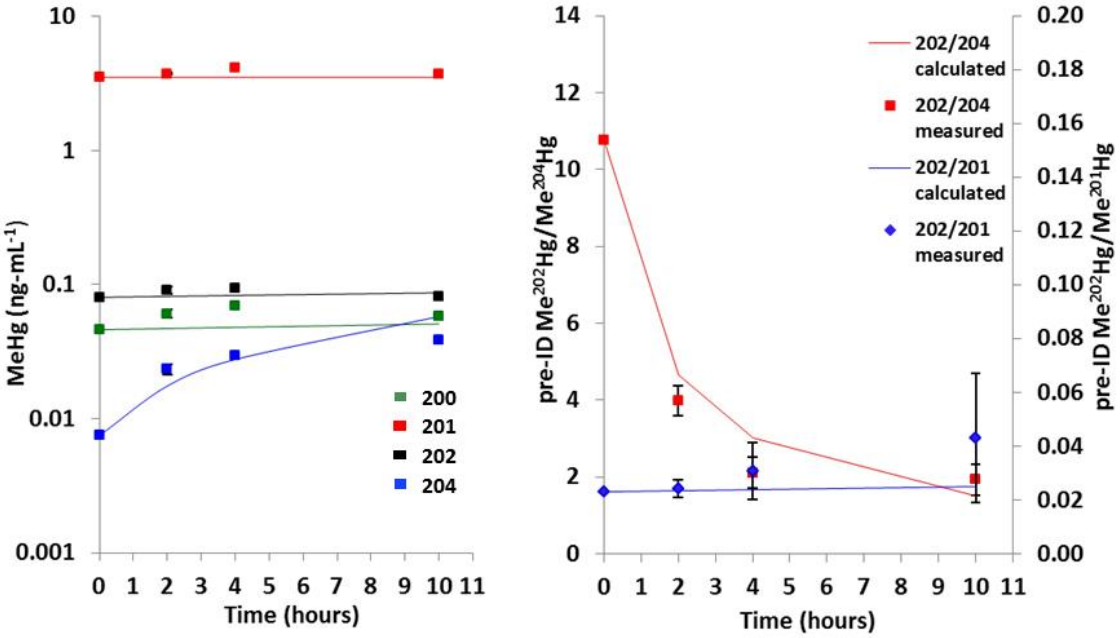

Figure 4. SSL ID-corrected concentration (left) and isotope ratio (right) measured data (points) and kinetic modeled values (lines) are displayed for a characteristic site A1 April 2012. Isotope ratio obtained k_{meth} = 2.0 E-4 hr^{-1} and k_{demeth} = 0 hr^{-1} rate constants were used to model both ID-corrected concentrations and isotope ratios. Error bars represent replicate analyses from same sample, and uncertainty for first time point calculated by error propagation. Logarithmic scale is used for ID-corrected concentrations to emphasize the greater fractional change of $Me^{204}Hg$ relative to other measured isotopes (200, 201, 202).

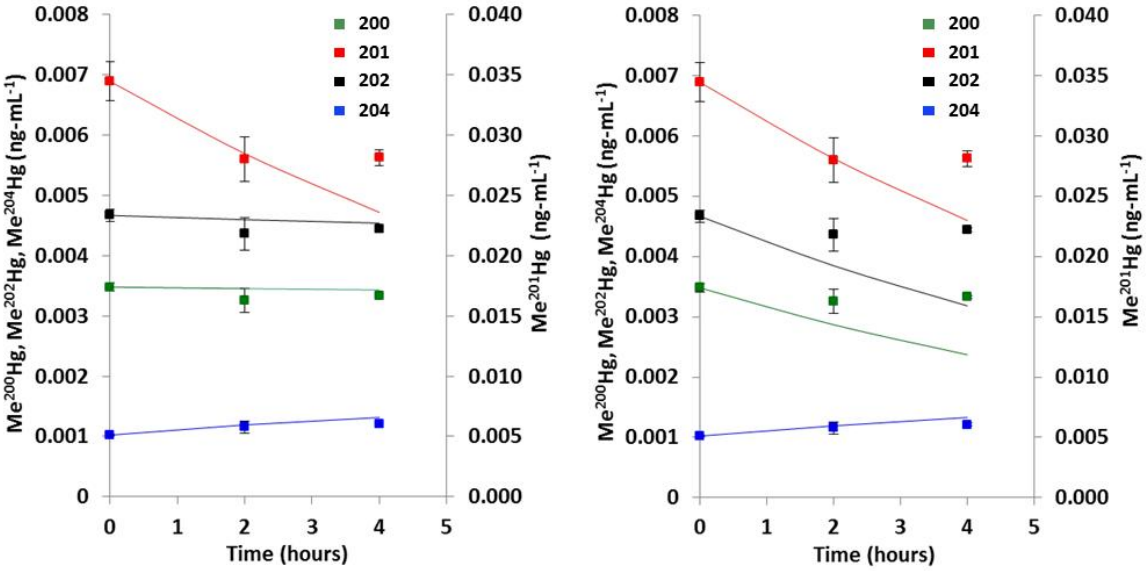

Figure 5. DBL ID-corrected concentrations (symbols) and kinetic modeled values (lines) are displayed for representative site A1 April 2012 for two cases: (left panel) shows model best fits assuming only the spike was bioavailable (yielding k_{meth} =9.54 E-4 hr^{-1}, k_{demeth} = 9.2 E-2 hr^{-1}); (right panel) shows model best fits assuming both ambient and spike were bioavailable (k_{meth} =2.0 E-3 hr^{-1}, k_{demeth} = 9.2 E-2 hr^{-1})). Error bars represent replicate analyses from same sample, and uncertainty for zero-time point calculated by error propagation.

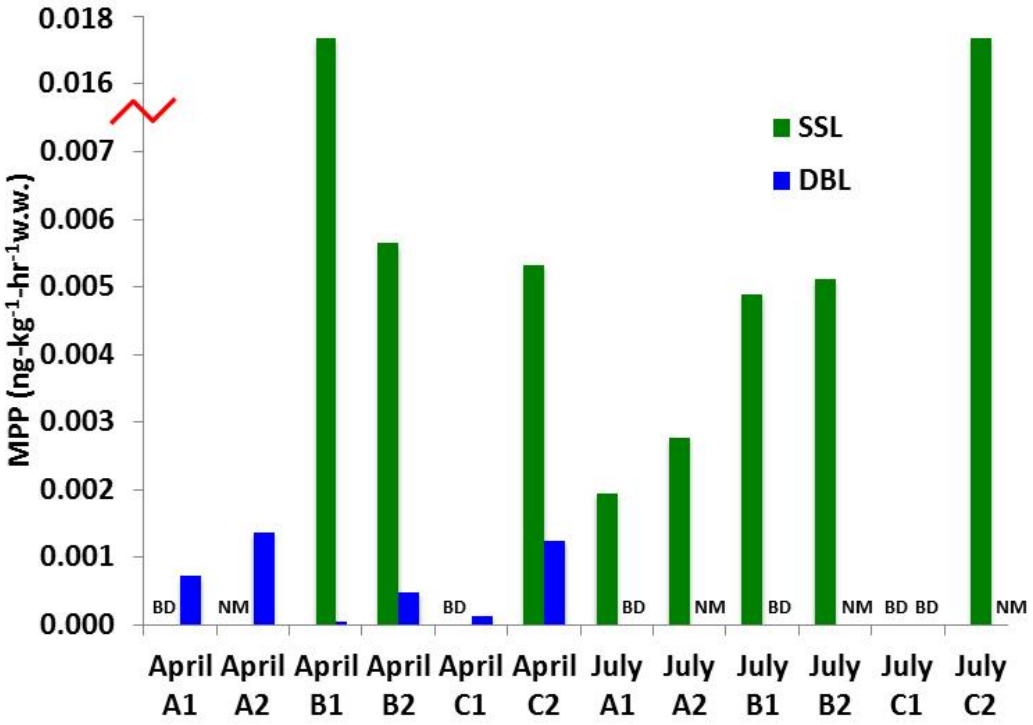

Figure 6. April (left) and July (right) MPPs (time-integrated product of k_{meth} and $Hg(II)_R$) for SSL and DBL. April SSL $Hg(II)_R$ concentrations at sites A1 and C1 were below detection limit (40.0 ng-kg^{-1} d.w.), and site A2 was not measured. July SSL $Hg(II)_R$ concentration at site C1 was below detection limit (30 ng-kg^{-1} d.w.). July DBL $Hg(II)_R$ concentrations were below detection limit (0.60 ng-L^{-1}) at all sites. SSL MPPs converted to wet weight rates for better comparison with DBL.

Table 2. Range of methylation (k_{meth}) and demethylation (k_{demeth}) rate constants for all locations.

		IMPOUNDED WETLANDS	FBN SUMMER	FBN FALL	OB	SSL APRIL	SSL JULY	DBL APRIL	DBL JULY
k_{meth} (hr^{-1})	LOW	1.0E-5	6.0E-6	1.4E-6	1.3E-4	1.1E-4	2.1E-5	3.6E-5	-
	HIGH	7.0E-5	2.1E-4	1.1E-3	5.4E-4	3.1E-4	1.5E-4	1.1E-3	1.1E-5
k_{demeth} (hr^{-1})	LOW					-	-	9.9E-2	3.0E-2
	HIGH					2.7E-2	1.9E-2	1.8E-1	5.0E-2

CHAPTER 4

DISCUSSION

4.1 DBL MeHg mitigation

Since the DBL has been implicated in the potential transfer of MeHg to the GSL ecosystem (Naftz et al., 2008), there has been informal consideration of strategies to mitigate MeHg production in the DBL. One potential strategy considered would be to aerate the DBL where it flows across a sill in the area between the north and central sampling transects as shown in Figure 1, and as measured (velocities) by the USGS (Dave Naftz, personal communication). This proposed strategy is sensible from the perspective that MeHg concentrations in the DBL are consistently high (in the range ~15-30 ng-L^{-1}, comprising ~40-60% of THg), and the conditions for mercury methylation are favorable in the DBL. However, this strategy assumes that the DBL is the primary source of MeHg. MPPs indicate otherwise (Figure 6), and point to the underlying SSL as a more potent source of MeHg relative to the DBL. Hence, aeration of the DBL at the sill seems unlikely to mitigate MeHg concentrations in the DBL. In fact, demethylation was a robust characteristic of the DBL as indicated by k_{demeth} values that were at minimum 2 orders of magnitude greater than k_{meth} values (Table 2); however, this comparison comes with a caveat that the "bioavailable" fractions of MeHg and IHg are not well constrained.

4.2 MeHg persistence in the DBL

That the DBL is not the predominant local source of MeHg makes unclear the reason why high MeHg concentrations (which generally fall between 15-30 ng-L^{-1}) persist in the DBL. Perhaps the SSL serves as a bottom boundary source of MeHg to the DBL. In which case, the question becomes whether the measured MeHg production from the SSL is sufficient to account for the observed MeHg concentrations in the DBL.

The change in MeHg concentration in the DBL is governed by MeHg production in both the SSL and DBL (the latter relatively negligible, but accounted for here), as well as MeHg removal from the DBL as shown below:

$$\frac{\partial [MeHg]_{DBL}}{\partial t} = \frac{MPP_{SSL} V_{SSL} \rho_{bSSL}}{V_{DBL}} + MPP_{DBL} - k_{demeth}[MeHg]_{DBL} \quad [6]$$

where: V_{DBL}, V_{SSL} are the volumes of the DBL and SSL, respectively, and ρ_{bSSL} is the bulk density of the SSL. The corresponding equation for the steady state MeHg concentration is:

$$[MeHg]_{DBL} = \frac{MPP_{SSL} V_{SSL} \rho_{b\,SSL}}{V_{DBL} k_{demeth}} + \frac{MPP_{DBL}}{k_{demeth}} \quad [7]$$

With respect to the parameters in equation 7, our study yielded average MPPs in the SSL and DBL during April 2012 (Table 3) of 9.3E-3 ng-kg^{-1}-hr^{-1} (wet weight) and 7.3E-4 ng-L^{-1}-hr^{-1}, respectively. The average k_{demeth} in the DBL during this period was 1.2E-1 hr^{-1}. Whereas the V_{SSL}:V_{DBL} ratio was not measured, we roughly estimated it to be 0.5. The value for ρ_{bSSL} was estimated to be 1.12 kg-L^{-1}. The resulting steady state MeHg concentration in the DBL is 5.0E-2 ng-L^{-1}, which is approximately 2.5 orders of magnitude smaller than the actual value (~15-30 ng-L^{-1}).

This discrepancy reflects the fact that (in equation 6) k_{demeth} acts upon the entire pool of MeHg in the DBL (necessitated by a lack of proxy for bioavailable MeHg).

In reality, it is unlikely that the entire pool of MeHg would be bioavailable. Furthermore, the laboratory condition in which demethylation was measured differed from *in situ* conditions lacking light. Provisional data from the USGS Lake Environmental Sensing Platform (Great Salt Lake Station 7.5 Miles West of Antelope Island) (http://waterdata.usgs.gov/ut/nwis/current/?type=flow) on the south arm of the GSL shows visible light decreases by a factor of ~4-7 between depths of 1.6 to 3.6 m, well above the upper boundary of the DBL (~6.5 m). Light penetration to the DBL is well known to be negligible due to high concentrations of dissolved and particulate organic matter (Supporting Information). Notably, UV light is attenuated more rapidly than visible light (Black, 2012). Our laboratory-measured k_{demeth} values decrease dramatically (0.123 hr^{-1} to 0.009 hr^{-1}) after 2 hours, which approximately corresponds to the time of light exposure during subsectioning in preparation for incubation. Visible light (e.g., 700-400 nm) has been shown to result in demethylation (Black, 2012).

In addition to light absorption, DOM may influence bioavailability. MeHg-DOM complexes have been shown to inhibit as well as promote biouptake depending on many not well constrained environmental factors (Dong, 2010). Although there is relatively little research on the effects of DOC on uptake of MeHg by microbes, it has been shown that higher DOC can inhibit uptake of MeHg of both freshwater (Gorski et al. 2006; Gorski et al. 2008) and marine alga (Zhong and Wang, 2009). In addition to DOM, the high sulfide concentrations in the DBL promote MeHg-S complexes (Hintelman et al., 1997) over MeHg-Cl complexes that are relatively bioavailable for uptake by alga (Zhong and Wang, 2009). High salinity levels (extreme in the DBL) have been shown to decrease photodemethylation. A salinity increase from 5 to 25 parts per thousand resulted

in 21% decrease in photodemethylation rate (Black, 2012). Extrapolating this decrease to the salinity levels of the DBL (e.g., 270 ppt) suggests a factor of two decrease in photodemethylation assuming a linear trend. That the ambient isotope MeHg concentrations do not track with the spiked $Me^{201}Hg$ isotope (Figure 5) (as mentioned above) supports the possibility that ambient MeHg is less available for demethylation relative to the $Me^{201}Hg$ spike. Assuming some degree of similarity between the processes governing MeHg and Hg(II) bioavailability, the low fraction of $Hg(II)_R$ relative to IHg(II) (3.9% ± 2.9%, n=6) in the DBL (see Supporting Information Table 4), suggests a potentially low fraction of bioavailable MeHg.

4.3 GSL system MeHg dynamics

The temporal decrease in MeHg concentrations in impounded wetlands sediment (75% of sites) and SSL (60% of sites) in 2012 (Figure 2) is unexplained, but may reflect a number of processes such as the influence of the spring snow-melt runoff bringing (for example) labile organic detritus and Hg(II) into the system. However, determination of this relationship is beyond the scope of this study. This temporal dynamic in MeHg concentrations, while it is likely not representative of other seasons or even other years, is important because it may influence temporal dynamics in the ecosystem. For example, eared grebes showed a temporal increase in blood Hg concentration from September to November 2006 of 5.6 ± 0.5 to 8.4 ± 1.2 $\mu g\text{-}g^{-1}$ (Conover and Vest, 2009b). This increase was interpreted to be related to residence time of eared grebes on the GSL. Our results demonstrate that, in addition to residence time, temporal variations in MeHg concentrations further contribute to the dynamics of the system.

Whereas distinction of the SSL vs. DBL as the predominant source of MeHg may or may not directly influence Hg uptake into the food web (a subject beyond the scope of this study), our finding of high MeHg concentrations in the sheet flow wetlands suggests the possibility of spatial "hot-spots" for MeHg introduction into the food web. While the biogeochemical drivers of the observed elevated MeHg concentrations in the sheet flow wetlands need further study, the need for such study is elevated by the fact that sheet flow wetlands provide an ideal habitat for macroinvertebrate populations that represent critical food sources for nesting and migratory shorebirds (Miller et al., 2009). Because the sheet flow wetlands are a nexus of ecosystem activity, they may be windows of Hg uptake into the greater ecosystem. Given the observed temporal dynamics in MeHg concentrations in the impounded wetlands (Figure 2), the temporal dynamics of the sheet flow wetlands should also be examined.

4.4 Parameters related to MeHg production

The observed spatial variation in MeHg concentrations (Figure 2) and mercury methylation rates (Table 2) warrant investigation to determine what parameters relate to this variability. The conditions governing Hg methylation are complex (Hsu-kim et al., 2013), but primarily involve SO_4^{2-} reduction as driven by the oxidation of labile organic carbon, indicating the possible correlation of (for example) MeHg concentration, or MeHg/THg, or k_{meth} with (for example) sulfide concentration and organic matter content. While SO_4^{2-} reduction is most closely associated with methylation (Compeau et al., 1985; Ranchou-Peyrouse et al., 2009), high sulfide concentrations may inhibit methylation by inhibiting the bioavailability of complexed Hg, depending on whether Hg is associated

with dissolved vs. nanoparticulate vs. microparticulate sulfide (Zhang et al., 2012; Gondikas et al., 2010; Gerbig et al., 2011; Hsu-kim et al., 2013).

To understand possible controls on MeHg production potential (MPP), correlations were examined between k_{meth} and our measured parameters. The statistically significant ($P < 0.05$) correlations are described below. Positive correlations were observed between k_{meth} values and sediment organic matter content in the freshwater influenced bays and impounded wetlands, as has been previously reported in other settings (Lambertsson and Nilsson, 2006; Marvin-Dipasquale et al., 2009). The methylation rate constants (k_{meth}) for two of the freshwater influenced bay transects (FBN summer, OB summer) and the impounded wetlands were significantly correlated ($P < 0.05$) to sediment organic matter content (Figure 7), with R^2 values of 0.895, 0.672, and 0.824, respectively. The corresponding 90% confidence intervals are provided for FBN summer, OBN summer, and the impounded wetlands in Figure 7. The FBN fall correlation had a relatively high R^2 of 0.879 but this correlation results from a single, high data point, and is not statistically significant with $P > 0.05$ ($P = 0.062$).

These correlations suggest an important role of sediment organic matter in regulating the production of MeHg in the freshwater influenced bays and impounded wetlands. However, when all the data from all locations are analyzed together, the correlation disappears, indicating that other factors in addition to sediment organic matter content (e.g., organic matter lability, sulfide concentrations, among others) influence the methylation rate constant. Whereas sediment organic matter content appears to influence methylation for a specific transect (area), other controlling factors must be identified in order to predict methylation rate constants across the larger system. The lack of

correlation between SSL k_{meth} and SSL organic matter content are unexplained, however, may be due to the minimal variation in SSL k_{meth} values measured.

Values of k_{meth} and $Hg(II)_R$ were negatively correlated in the SSL ($R^2 = 0.999$, April; $R^2 = 0.447$, July; $R^2 = 0.386$, combined), with the April correlation being significant ($P < 0.05$), the July correlation being not statistically significant ($P = 0.22$), and the combined correlation being marginally significant ($P = 0.10$) (Figure 8). Notably, these negative correlations yielded similar MPPs in the SSL across April and July despite large variation in k_{meth} and $Hg(II)_R$ values across those two months. Recall that MPP is the time-integrated product of k_{meth} and $Hg(II)_R$. In contrast to the SSL, the DBL showed greatly reduced MPPs in July relative to April because both k_{meth} and $Hg(II)_R$ decreased together (positively correlated) during this period. It is striking that the observed MeHg concentrations are temporally constant in the DBL despite its MPP values having high temporal variation (Figure 6). The temporally constant MPPs in the SSL therefore seem to link methylation in the SSL with high and constant MeHg values in the DBL, and further indicate the SSL as the predominant source of MeHg in the DBL. Whereas the negative correlation between k_{meth} and $Hg(II)_R$ is highly dependent on a single high $Hg(II)_R$ value (Figure 8), the dominance of the SSL relative to the DBL (in terms of MPP) remains even in the absence of this value (Figure 6).

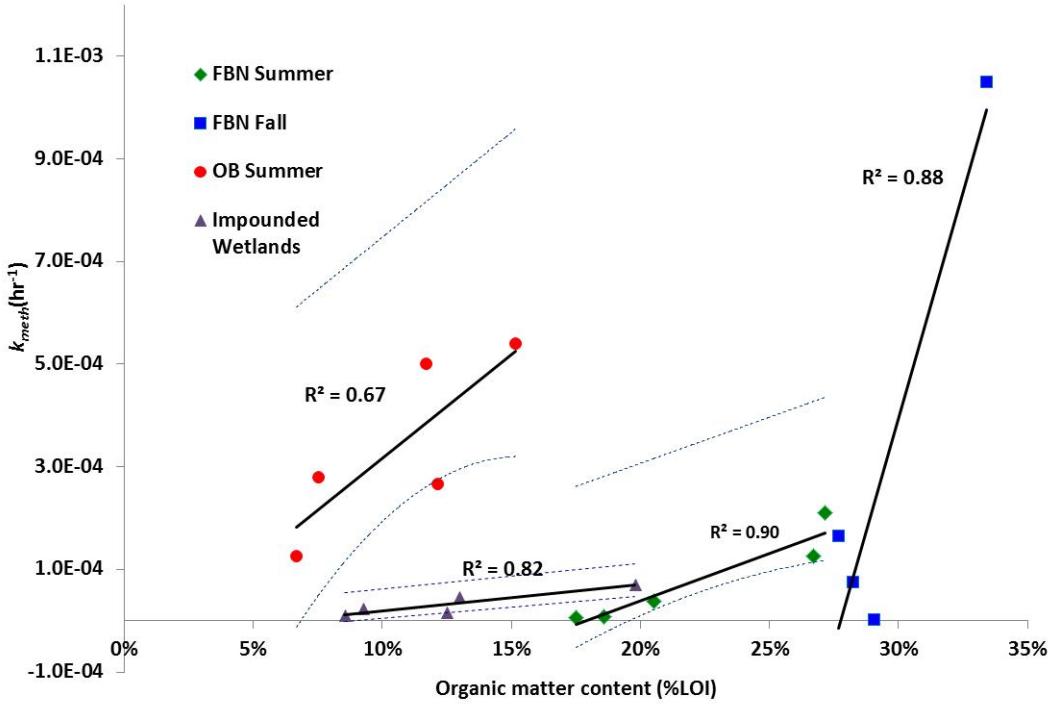

Figure 7. Scatter plots of methylation rate constants (k_{meth}) (hr^{-1}) vs. percent sediment organic matter content (%LOI) in sediment from the freshwater bays (summer and fall 2009) and impounded wetlands (summer 2011) with trend lines and R^2 values included. Dashed lines represent 90% confidence intervals.

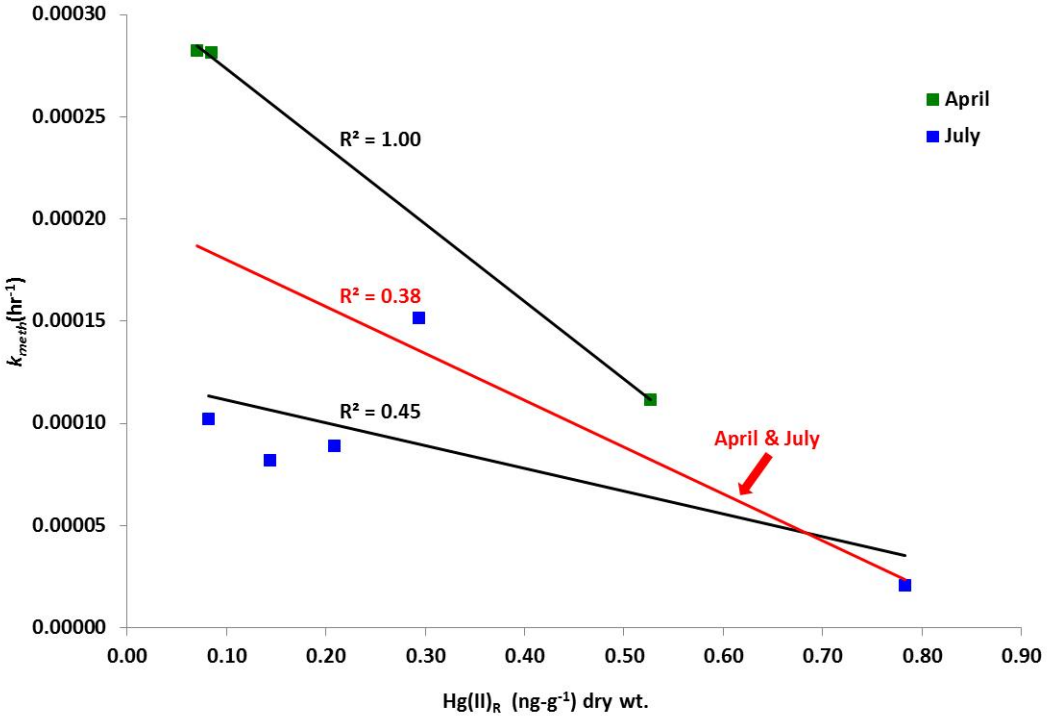

Figure 8. Scatter plots of SSL methylation rate constants (k_{meth}) (hr^{-1}) vs. Hg(II)$_R$ (ng-g^{-1}) for April and July of 2012. Trend lines and R^2 values included. Combined April and July data represented by red trend line.

Table 3. April and July MPPs represented by k_{meth} calculated from ID corrected concentration changes and the concentration of $Hg(II)_R$. April SSL $Hg(II)_R$ concentrations at sites A1 and C1 were below detection limit (40.0 ng-kg^{-1} d.w.), and site A2 was not measured. July SSL $Hg(II)_R$ concentration at site C1 was below detection limit (30 ng-kg^{-1} d.w.). July DBL $Hg(II)_R$ concentrations were below detection limit (0.60 ng-L^{-1}) at all sites. SSL MPPs converted to wet weight rates for better comparison with DBL.

Date	Sample Media	Sample	MPP	MPP
	DBL		ng-kg^{-1}-hr^{-1}	ng-L^{-1}-hr^{-1}
Apr-12		A1	7.1-04	8.0-04
Jul-12		A1	-	-
Apr-12		A2	1.4E-03	1.5E-03
Apr-12		B1	4.3E-05	4.8E-05
Jul-12		B1	-	-
Apr-12		B2	4.7E-04	5.2E-04
Apr-12		C1	1.1E-04	1.3E-04
Jul-12		C1	-	-
Apr-12		C2	1.2E-03	1.4E-03
	SSL		ng-kg^{-1}-hr^{-1}	
Apr-12		A1	-	
Jul-12		A1	1.9E-03	
Jul-12		A2	2.8E-03	
Apr-12		B1	1.7E-02	
Jul-12		B1	4.9E-03	
Apr-12		B2	5.6E-03	
Jul-12		B2	5.1E-03	
Apr-12		C1	-	
Jul-12		C1	-	
Apr-12		C2	5.3E-03	
Jul-12		C2	1.7E-02	

CHAPTER 5

CONCLUSION

The GSL is an important ecosystem for millions of migratory birds with over 1.4 million shorebirds using the GSL and surrounding wetlands for breeding and staging areas (Aldrich and Paul, 2002). High and spatially constant MeHg concentrations (~15-30 ng-L^{-1}) in the DBL of the GSL could potentially provide for the transfer of MeHg to the GSL ecosystem. However, entry of MeHg into the ecosystem may not be related to the DBL, but rather may occur within the freshwater wetlands on the eastern boundary of the GSL. The highest concentrations of MeHg in water and sediment were found in the south arm of the GSL and the sheetflow wetlands, representing possible "hot-spots" for MeHg introduction into the food web.

Positive correlation of k_{meth} to organic matter content was observed in sediment of the freshwater influenced bays and impounded wetlands, while this trend was not observed in DBL and SSL of the GSL. These results further indicate that sediment organic matter, as well as other factors (e.g., organic matter lability and sulfide concentrations) contribute to production of MeHg.

Favorable conditions for mercury methylation and consistently high MeHg concentrations in the DBL (in the range ~15-30 ng-L^{-1}, comprising ~40-60% of Hg) (Figure 1), suggest the possibility that MPPs are exceptionally high in this system relative

to other settings. However, MPPs in the SSL were found to be lower than MPPs found in sediments from a variety of wetland settings (Windham-Myers et al., 2010), and bracketed by MPPs in sediments from diverse stream environments (Marvin-DiPasquale et al., 2009). MPP values in the DBL were at, or below, the low end for sediments from these stream environments. This comparison demonstrates that the MPPs from the DBL and SSL are not high relative to other settings.

To explain the high MeHg concentrations in the DBL, its inherent characteristics likely inhibit demethylation. We therefore conclude that the high MeHg concentrations in the DBL result from lack of demethylation via the lack of light penetration, high salinity, abundance of dissolved and particulate organic matter, and other biogeochemical factors.

APPENDIX A

TOTAL, METHYL, AND "REACTIVE" INORGANIC MERCURY DATA

A.1 Total and methyl mercury concentrations

Table 4. Freshwater impounded and sheet flow wetlands THg and MeHg concentration averages, standard deviation, and samples analyzed (n).

Location	Sample Media	Sample	THg ($ng\text{-}L^{-1}$)	Standard Deviation	MeHg ($ng\text{-}L^{-1}$)	Standard Deviation	n
Wetlands							
	Surface Water						
		GSL-008	0.806	0.13	0.163	0.028	2
		GSL-011	0.937	0.05	0.101	0.072	2
		GSL-010	0.910	0.42	0.115		1
		GSL-014	1.141	0.13	0.167	0.205	2
		GSL-017	0.996	0.00	0.035	0.035	2
		NS 47	0.592	0.23	0.052	0.043	8
		GSL-019	0.931	0.54	0.025	0.009	2
		GSL-022	1.034	0.49	0.037	0.036	2
		GSL-013	0.894	0.36	0.042	0.015	2
		GSL-012	1.120	0.37	0.075	0.011	2
		FB1	0.577	0.24	0.099	0.076	12
		FB2	1.143	0.34	0.358	0.313	11
		W1	0.744	0.28	0.076	0.081	12
		PINTAIL	1.002	0.36	0.096	0.130	12
		BR-5C	2.377	0.05	0.476	0.447	2
		BR-4C	1.756	0.31	0.228	0.172	3
		GSL-009	1.365	0.28	0.225	0.127	4
Location	Sample Media	Sample	THg ($ng\text{-}L^{-1}$)	Standard Deviation	MeHg ($ng\text{-}L^{-1}$)	Standard Deviation	n
	Pore Water						
		W1	1.421	0.730	0.063	0.045	15
		NS 47	1.54	0.48	0.096	0.062	15
		FB1	1.46	0.79	0.077	0.053	17
		FB2	1.65	0.72	0.075	0.076	17
		PINTAIL	2.56	0.56	0.095	0.104	11
		CD-1	5.29	0.42	0.919	0.310	3
		CD2	8.09	2.87	3.747	2.652	3
		CD3	29.73	7.81	5.345	2.468	3
		KC-1	2.44	0.47	0.677	0.058	3
		KC-3	38.33	39.55	12.153	16.155	3
Location	Sample Media	Sample	THg ($ng\text{-}kg^{-1}$)	Standard Deviation	MeHg ($ng\text{-}kg^{-1}$)	Standard Deviation	n
	Sediment						
		GSL-008	247675	20908	93.2	0.1	2
		GSL-011	44774	2784	58.5	29.4	2
		GSL-010	42115	6446	19.2	5.0	2
		GSL-014	108743	1737	117.4	120.8	2
		GSL-017	148300	10491	100.4	49.1	2
		NS 47	191199	16051	115.7	19.9	4
		GSL-019	171894	85660	73.9	29.2	2
		GSL-022	67259	16185	288.3	147.3	2
		GSL-013	302017	11074	98.3	46.2	2
		GSL-012	31716	876	50.4	53.8	2
		FB1	139631	46587	60.1	48.9	8

Table 4. Continued.

Location	Sample Media	Sample	THg ($ng\text{-}L^{-1}$)	Standard Deviation	MeHg ($ng\text{-}L^{-1}$)	Standard Deviation	n
		FB2	147279	28597	58.4	48.8	8
		W1	137187	17959	42.8	36.5	8
		PINTAIL	15365	5287	20.1	16.6	8
		FB1	139631	46587	60.1	48.9	8
		FB2	147279	28597	58.4	48.8	8
		W1	137187	17959	42.8	36.5	8
		PINTAIL	15365	5287	20.1	16.6	8
		BR 5C	24121	3932	501.1	159.1	2
		BR 4C	32248	3810	87.5	67.2	3
		GSL-009	129009	9209	98.0	101.3	4
		CD-1	331994		292.2		1
		CD-2	251021		978.4		1
		CD-3	348576		948.4		1
		KC-1	34365		185.3		1
		KC-3	150234		494.7		1

Table 5. GSL THg and MeHg concentration averages, standard deviation, and samples analyzed (n).

Sample Media	Sample	THg ($ng\text{-}L^{-1}$)	Standard Deviation	MeHg ($ng\text{-}L^{-1}$)	Standard Deviation	n
DBL						
	A1	54.4	13.6	21.4	9.9	2
	A2	39.9	2.6	21.7	6.3	2
	A3	38.7		23.2		1
	B1	55.4	8.9	29.1	4.1	3
	B2	53.2	8.0	23.3	8.6	2
	B3	38.2		29.4		1
	C1	64.1	33.6	21.5	9.9	3
	C2	64.6	25.2	20.8	6.0	2
Sample Media	Sample	THg ($ng\text{-}kg^{-1}$)	Standard Deviation	MeHg ($ng\text{-}kg^{-1}$)	Standard Deviation	n
SSL						
	A1	48094	6.68E+03	482	250	2
	A2	64337		655		1
	B1	242752	6.50E+04	1603	267	2
	B2	149955.5	3.83E+04	1462	113	2
	C1	31550	6.84E+03	437	56	2
	C2	81293.5	3.82E+04	490	348	2

Table 6. Freshwater influenced bays THg and MeHg concentration averages, standard deviation, and samples analyzed (n).

Location	Sample Media	Sample	THg ($ng\text{-}L^{-1}$)	Standard Deviation	MeHg ($ng\text{-}L^{-1}$)	Standard Deviation	n
Bays							
	Surface Water						
		FBN-1	16.6	9.7	4.94	6.02	2
		FBN-2	9.7	3.7	1.04	0.60	2
		FBN-3	8.1	0.6	1.32	0.38	2
		FBN-4	7.1	0.7	0.90	0.08	2
		FBN-5	9.0		1.64		1
		FBS-1	72.2		1.11		1
		FBS-2	170.0		0.19		1
		FBS-3	6.3		1.85		1
		FBS-4	11.9		0.09		1
		FBS-5	47.3		0.23		1
		OB-1	7.3		0.53		1
		OB-2	12.1		0.73		1
		OB-3	19.8		1.10		1
		OB-4	11.4		0.31		1
		OB-5	24.8		0.65		1
	Sample Media	Sample	THg ($ng\text{-}kg^{-1}$)	Standard Deviation	MeHg ($ng\text{-}kg^{-1}$)	Standard Deviation	n
	Sediment						
		FBN-1	5575	389	27	16	2
		FBN-2	8070	410	11	6	2
		FBN-3	10480	5261	44	33	2
		FBN-4	11855	14064	26	33	2
		FBN-5	58800		319		1
		FBS-1	180500	75660	115	145	2
		FBS-2	250500	65761	226	122	2
		FBS-3	51300	47659	134	44	2
		FBS-4	66500	10041	19	18	2
		FBS-5	67550	17607	54	23	2
		OB-1	33300		311		1
		OB-2	13700		168		1
		OB-3	38200		203		1
		OB-4	24800		408		1
		OB-5	20000		75		1

A.2 "Reactive" inorganic mercury concentrations

Table 7. $Hg(II)_R$ and $\%Hg(II)_R$ of IHg (calculated as THg-MeHg) for DBL and SSL of GSL, summer 2012.

Location	Date	Sample Media	Sample	$Hg(II)_R$	% $(Hg(II)_R\text{-}IHg^{-1})$
GSL					
		DBL		$ng\text{-}L^{-1}$	
	Apr-12		A1	1.07	3.5
	Jul-12		A1	<0.60	-
	Apr-12		A2	1.97	9.4
	Apr-12		B1	1.33	4.3
	Jul-12		B1	<0.60	-
	Apr-12		B2	1.00	2.4
	Apr-12		C1	1.58	1.9
	Jul-12		C1	<0.60	-
	Apr-12		C2	1.29	2.0
		SSL		$ng\text{-}kg^{-1}$ d.w.	
	Apr-12		A1	<40	-
	Jul-12		A1	80	0.19
	Jul-12		A2	140	0.23
	Apr-12		B1	520	0.18
	Jul-12		B1	780	0.40
	Apr-12		B2	80	0.07
	Jul-12		B2	210	0.12
	Apr-12		C1	<40	-
	Jul-12		C1	<30	-
	Apr-12		C2	70	.13
	Jul-12		C2	290	0.27

APPENDIX B

ISOTOPE TRACERS AND ISOTOPE DILUTION SPIKE DATA

Table 8. Isotope tracer ($I^{204}Hg$ and $Me^{201}Hg$) and isotope dilution ($Me^{200}Hg$) spike percentages relative to ambient mercury concentrations.

GSL Deep Brine Layer (DBL)

	A1 DBL	A1 DBL	A2 DBL	B1 DBL	B1 DBL	B2 DBL	C1 DBL	C1 DBL	C2 DBL
Month	APRIL	JULY	APRIL	APRIL	JULY	APRIL	APRIL	JULY	APRIL
I204Hg	197%	138%	236%	158%	140%	152%	115%	338%	140%
Me201Hg	230%	116%	196%	131%	100%	195%	182%	265%	210%
Me200Hg	208%	105%	174%	117%	89%	174%	157%	230%	181%

GSL Sediment Slurry (SSL)

	A1 SSL	A1 SSL	A2 SSL	B1 SSL	B1 SSL	B2 SSL	B2 SSL	C1 SSL	C1 SSL	C2 SSL	C2 SSL
Month	APRIL	JULY	JULY	APRIL	JULY	APRIL	JULY	APRIL	JULY	APRIL	JULY
I204Hg	208%	98%	66%	97%	135%	299%	62%	875%	139%	576%	35%
Me201Hg	1148%	24%	24%	465%	61%	637%	52%	2131%	42%	3648%	54%
Me200Hg	174%	24%	24%	86%	61%	82%	48%	2188%	31%	540%	54%

Freshwater Influenced Bays

	FBNS1	FBNS2	FBNS3	FBNS4	FBNS5	FBNF1	FBNF2	FBNF3	FBNF4
Month	July	July	July	July	July	October	October	October	October
I204Hg	57%	39%	21%	14%	5%	125%	87%	108%	38%

	OBS1	OBS2	OBS3	OBS4	OBS5
Month	July	July	July	July	July
I204Hg	81%	198%	71%	110%	136%

Impounded Wetlands

	W-1	N47	FB-1	FB-2	Pintail
Month	August	August	August	August	August
I204Hg	18%	13%	18%	17%	164%

APPENDIX C

KINETIC MODELING DATA

C. 1 Compiled rate constants

Table 9. Methylation (k_{meth}) and demethylation (k_{demeth}) rate constants for all GSL samples

Location	Date	Sample Media	Sample	k_{meth} hr^{-1}	k_{demeth} hr^{-1}
GSL					
		DBL			
	Apr-12		A1	7.50E-04	1.10E-01
	Jul-12		A1	1.10E-05	3.80E-02
	Apr-12		A2	7.80E-04	1.00E-01
	Apr-12		B1	3.60E-05	1.30E-01
	Jul-12		B1	-	3.00E-02
	Apr-12		B2	5.20E-04	1.20E-01
	Apr-12		C1	8.20E-05	1.80E-01
	Jul-12		C1	-	5.00E-02
	Apr-12		C2	1.10E-03	9.90E-02
		SSL			
	Apr-12		A1	3.10E-04	-
	Jul-12		A1	1.00E-04	-
	Jul-12		A2	8.20E-05	-
	Apr-12		B1	1.10E-04	-
	Jul-12		B1	2.10E-05	1.90E-02
	Apr-12		B2	2.80E-04	-
	Jul-12		B2	8.90E-05	-
	Apr-12		C1	1.30E-04	2.70E-02
	Jul-12		C1	-	-
	Apr-12		C2	2.80E-04	-
	Jul-12		C2	1.50E-04	-

Table 10. Methylation (k_{meth}) and demethylation (k_{demeth}) rate constants for freshwater influenced bay sediment samples.

Location	Date	Sample Media	Sample	k_{meth} hr^{-1}	k_{demeth} hr^{-1}
Freshwater Influenced Bays					
		Sediment			
	Jul-09		FBN-1	1.10E-03	-
	Oct-09		FBN-1	2.10E-04	-
	Jul-09		FBN-2	7.50E-05	-
	Oct-09		FBN-2	3.80E-05	-
	Jul-09		FBN-3	1.70E-04	-
	Oct-09		FBN-3	6.00E-06	-
	Jul-09		FBN-4	1.40E-06	-
	Oct-09		FBN-4	1.30E-04	-
	Oct-09		FBN-5	7.00E-06	-
	Aug-10		OB-1	1.30E-04	-
	Aug-10		OB-2	5.40E-04	-
	Aug-10		OB-3	2.70E-04	-
	Aug-10		OB-4	5.00E-04	-
	Aug-10		OB-5	2.80E-04	-

Table 11. Methylation (k_{meth}) and demethylation (k_{demeth}) rate constants for impounded wetland sediment samples.

Location	Date	Sample Media	Sample	k_{meth} hr^{-1}	k_{demeth} hr^{-1}
Impounded Wetlands					
		Sediment			
	Aug-10		AMDCW	1.60E-05	-
	Aug-10		N47	1.00E-05	-
	Aug-10		FB1	4.50E-05	-
	Aug-10		FB2	7.00E-05	-
	Aug-10		PINTAIL	2.30E-05	-

C. 2 GSL kinetic modeling

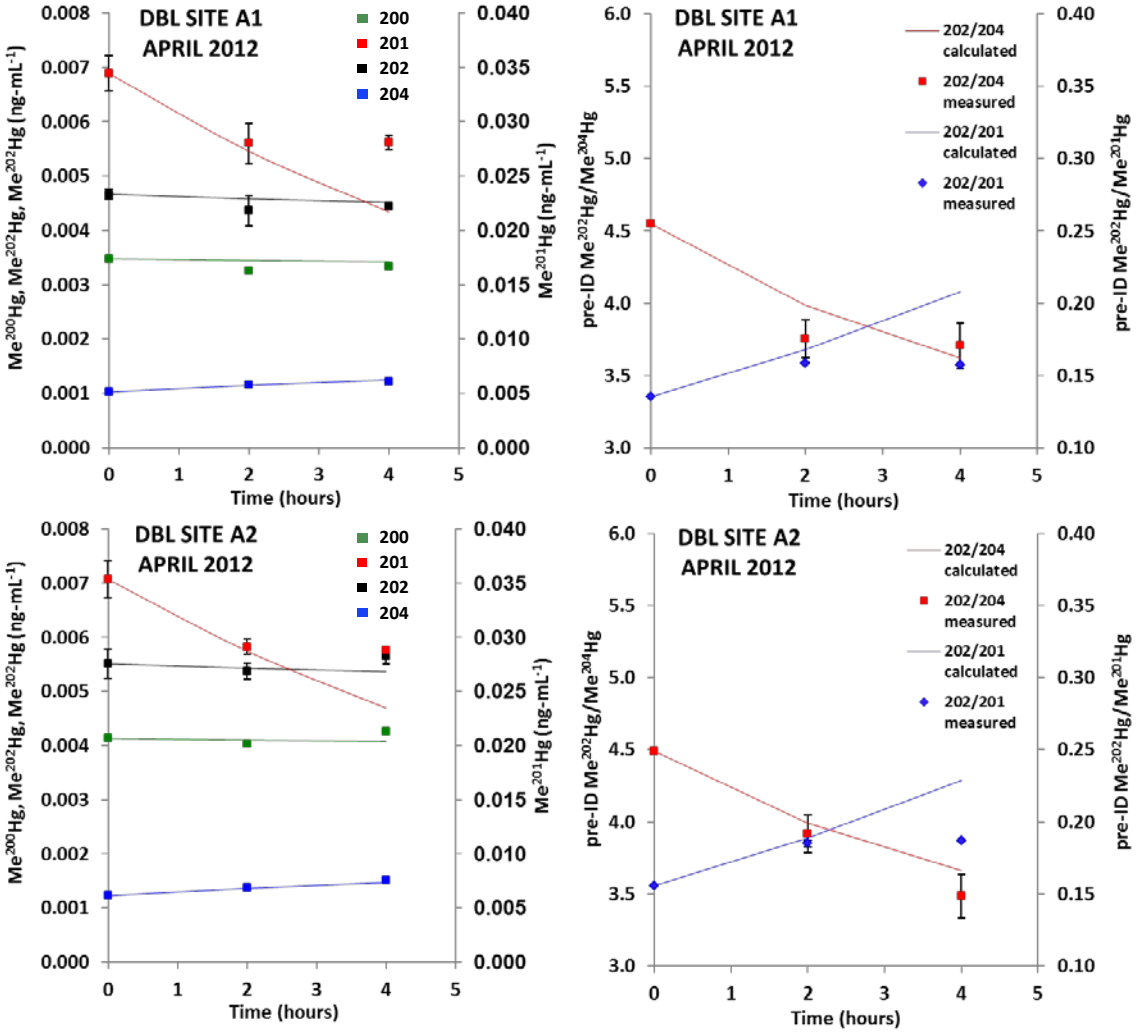

Figure 9. ID-corrected concentration (left) and isotope ratio (right) measured data (points) and kinetic modeled values (lines) are displayed for all DBL sites and dates (April and July 2012), and sampling locations. Error bars represent replicate analyses from same sample, and uncertainty for first time point calculated by error propagation.

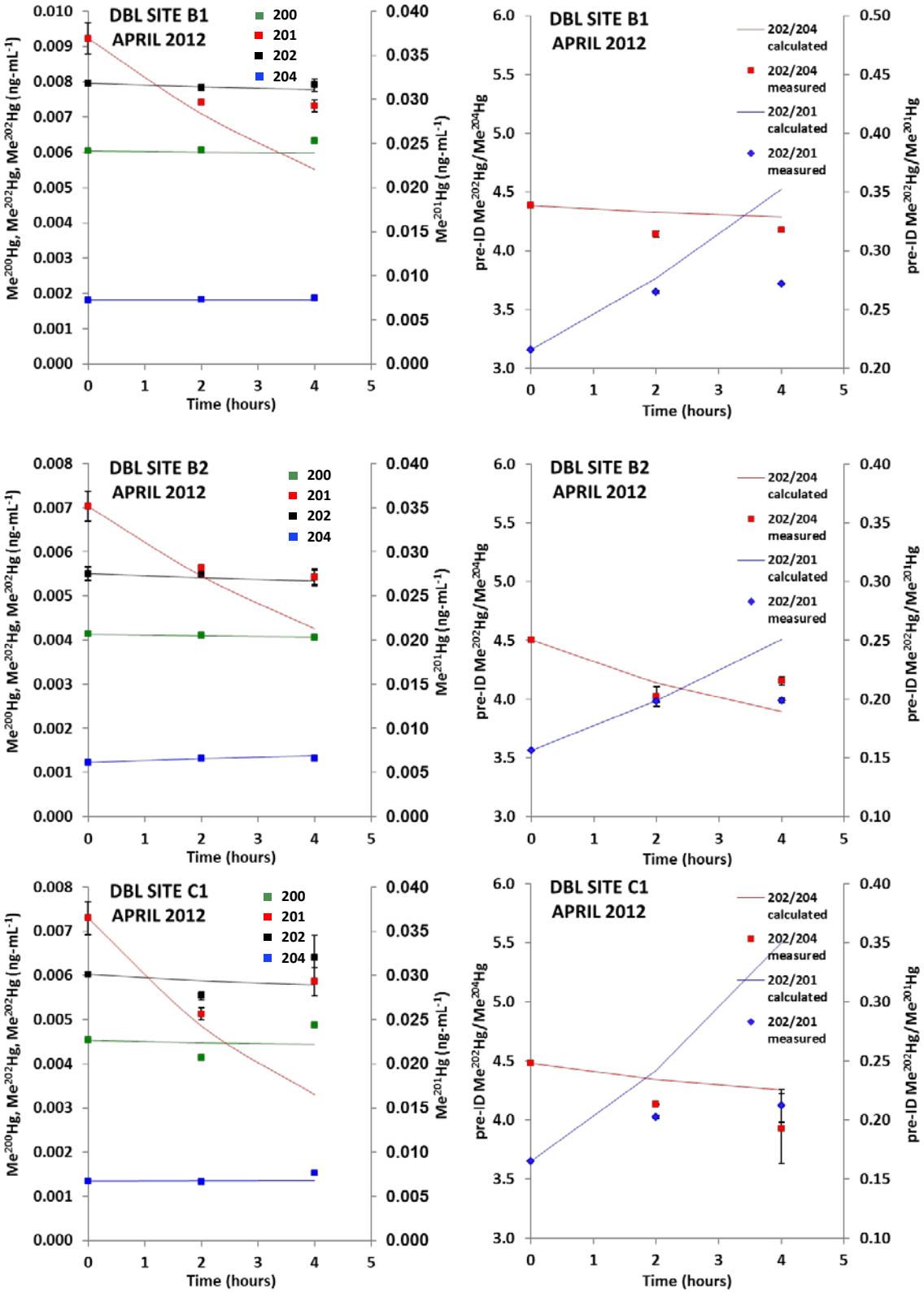

Figure 9. Continued.

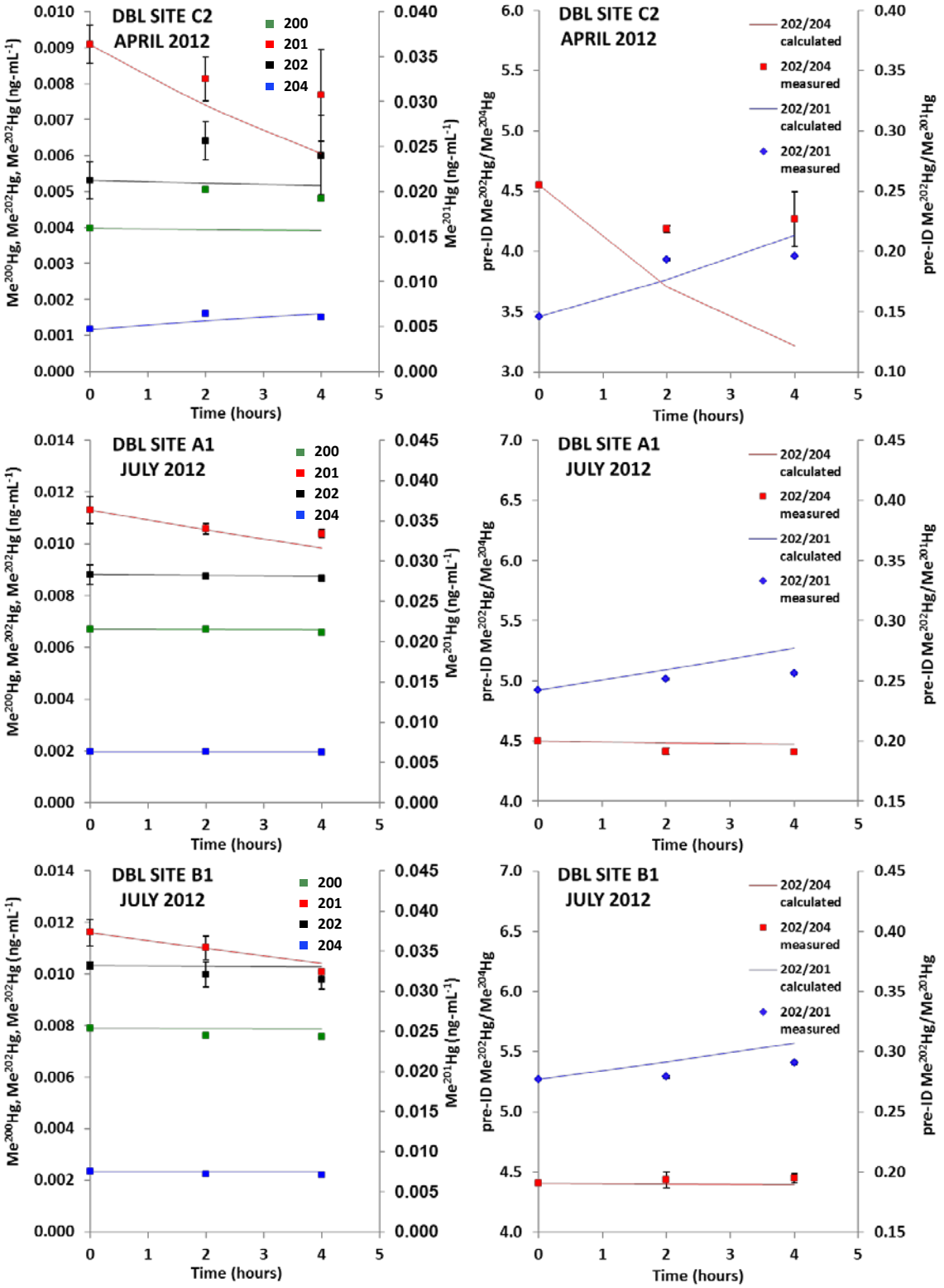

Figure 9. Continued.

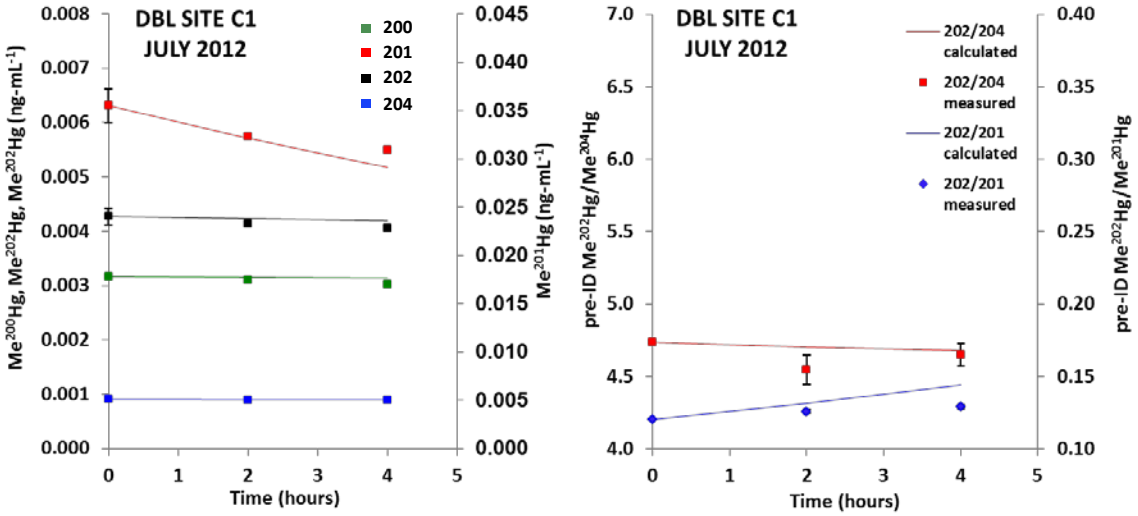

Figure 9. Continued.

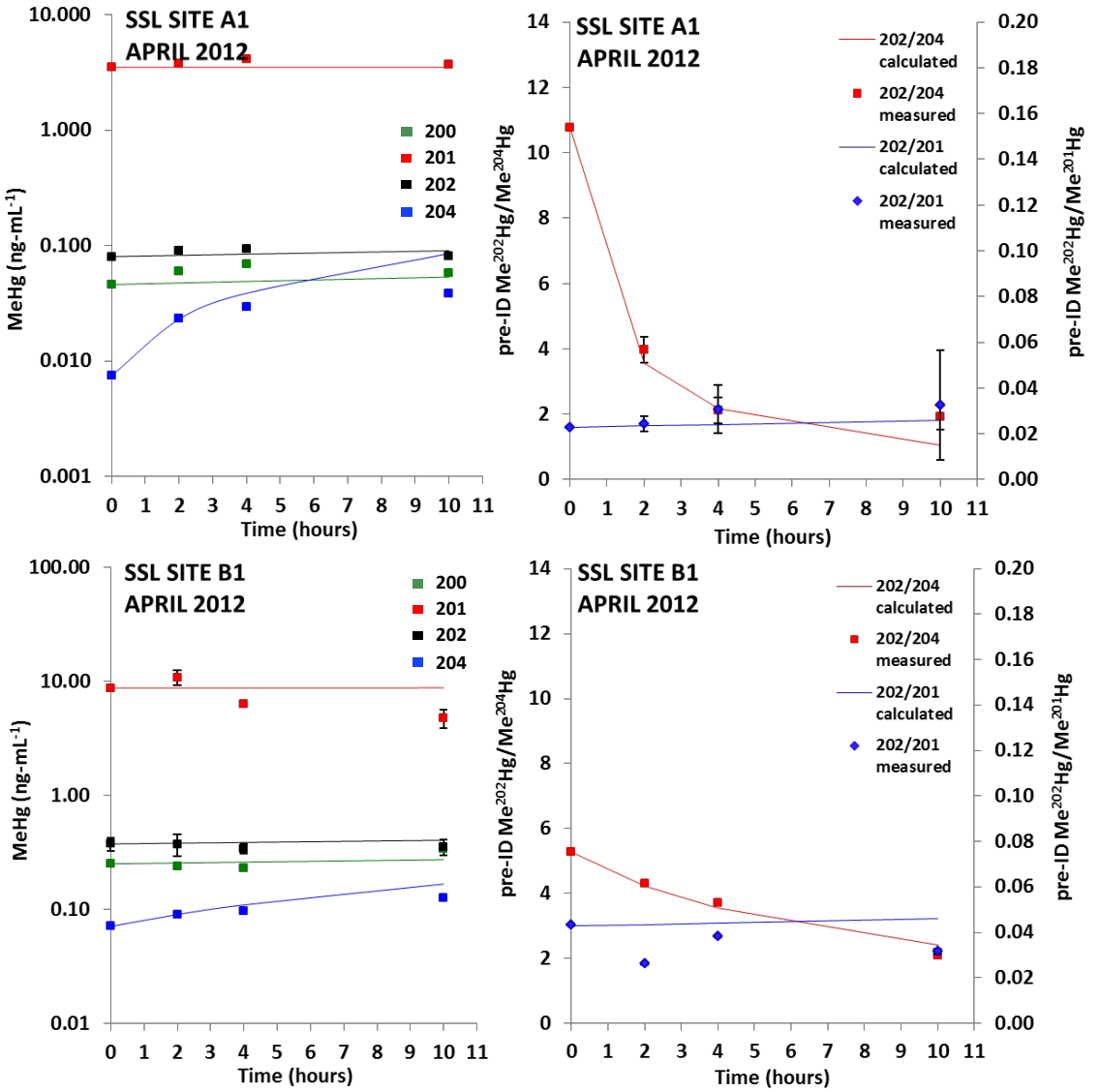

Figure 10. ID-corrected concentration (left) and isotope ratio (right) measured data (points) and kinetic modeled values (lines) are displayed for all SSL sites and dates (April and July 2012), and sampling locations. Error bars represent replicate analyses from same sample, and uncertainty for first time point calculated by error propagation. Logarithmic scale is used for ID-corrected concentrations to emphasize the greater fractional change of $Me^{204}Hg$ relative to other measured isotopes in April SSL samples, whereas linear scale is used for July SSL due to a smaller absolute change of $Me^{204}Hg$.

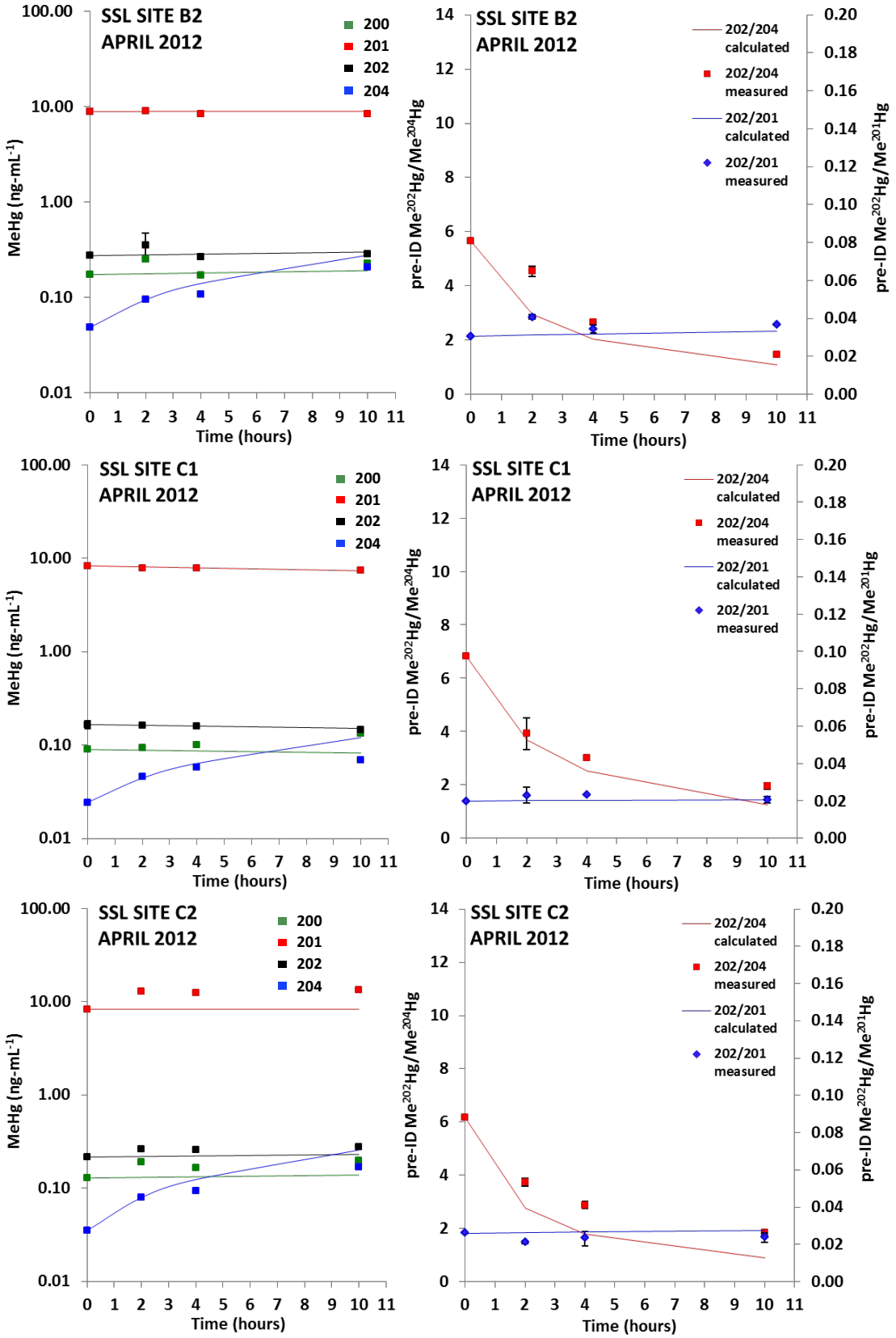

Figure 10. Continued.

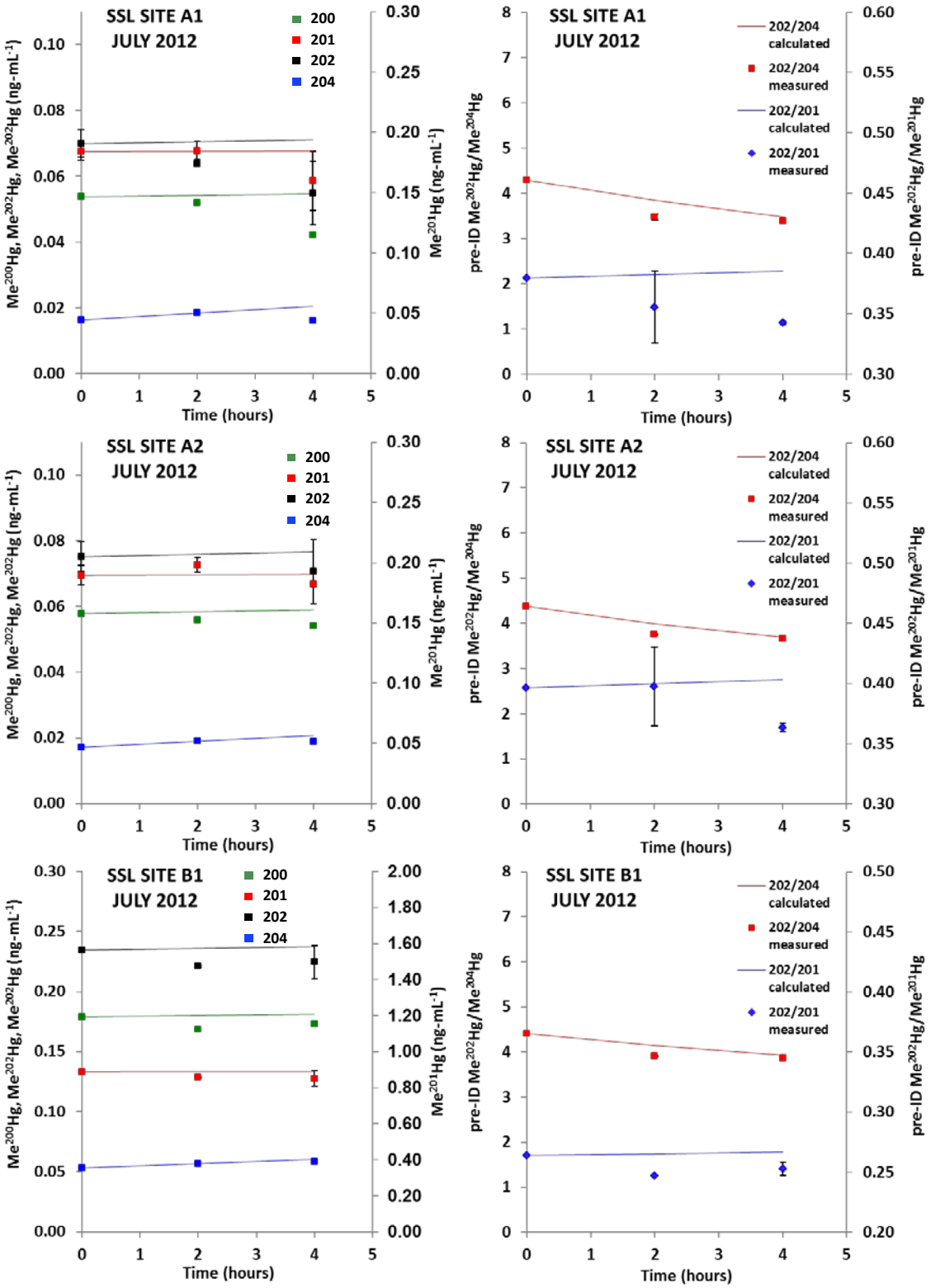

Figure 10. Continued.

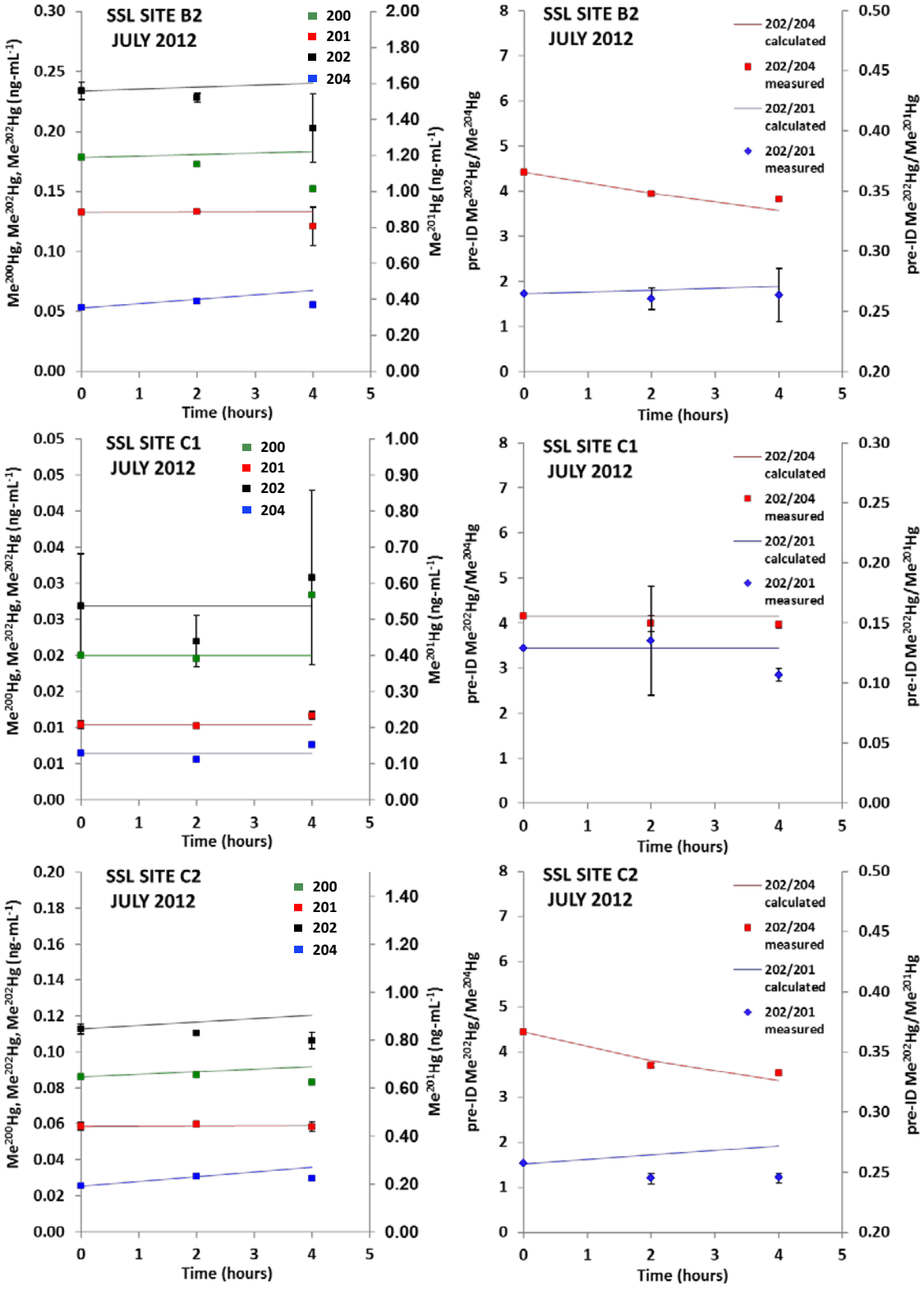

Figure 10. Continued.

APPENDIX D

DEEP BRINE LAYER SUPPLEMENTARY DATA

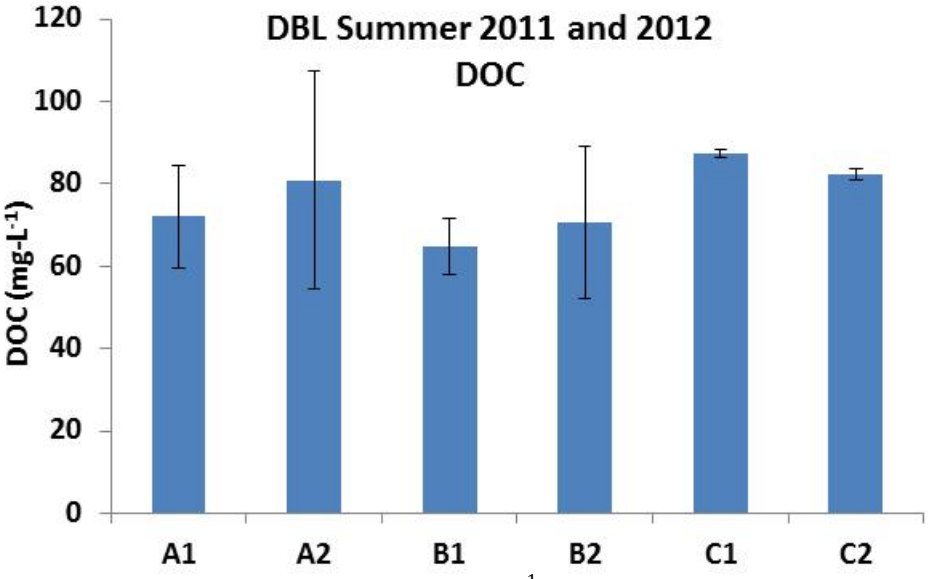

Figure 11. Column plot of DOC (mg-L^{-1}) from DBL of the GSL. Summer 2011 and 2012 data were averaged for each respective site.

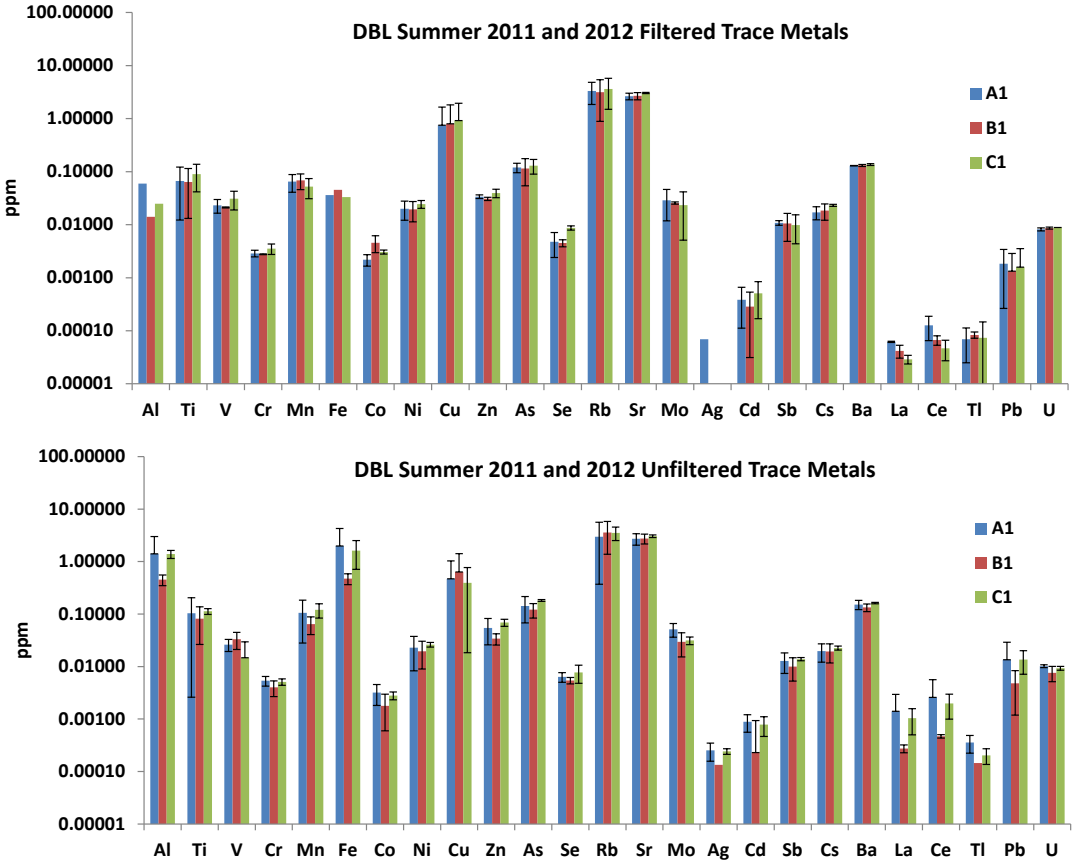

Figure 12. Column plot of filtered (top) and unfiltered (bottom) trace element data from DBL (sites A1, B1, and C1 averaged) of the GSL. Summer 2011 and 2012 data were averaged for each respective site. Al and Fe were under detection limit in filtered samples from 2012, 0.01 ppm and 0.2 ppm, respectively. Ag was under detection limit at all but one site (A1) in 2012 (DL = 0.0001 ppm) and all sites in 2011 (DL= 0.0001 ppm).

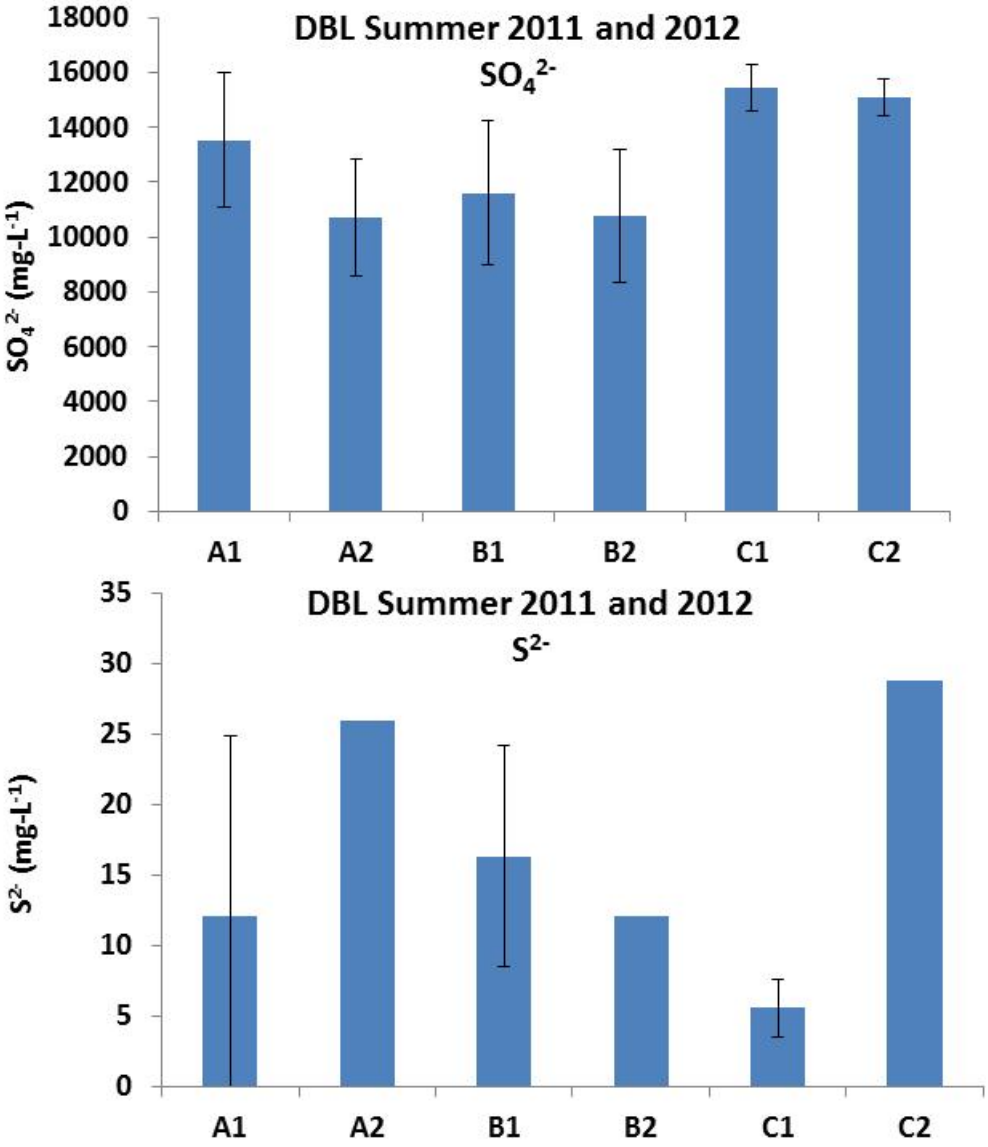

Figure 13. Column plot of $SO4^{2-}$ (mg-L^{-1}) and S^{2-} (mg-L^{-1}) from DBL of the GSL. Summer 2011 and 2012 data averaged for each respective site.

REFERENCES

Aldrich TW, Paul DS. Avian ecology of Great Salt Lake in Gwynn, J.W., ed. Great Salt Lake: an overview of change. Utah Department of Natural Resources Special Publication 2002;343-74.

Baeyens W, Leermakers M, Papina T, Saprykin A, Brion N, Noyen J et al. Bioconcentration and biomagnification of mercury and methylmercury in North Sea and Scheldt estuary fish. Arch Environ Contam Toxicol 2003;45:498-508.

Benoit JM, Gilmour CC, Mason RP, Heyes A. Sulfide controls on mercury speciation and bioavailability to methylating bacteria in sediment pore waters. Environ Sci Technol 1999;33:951-7.

Black FJ, Poulin BA, Flegal AR. Factors controlling the abiotic photo-degradation of monomethylmercury in surface waters. Geochemica et Cosmochimica Acta 2012; 84:492-507.

Bloom NS, Colman JA, Barber L. Artifact formation of methyl mercury during aqueous distillation and alternative techniques for the extraction of methyl mercury from environmental samples. Fresenius J Anal Chem 1997;358:371-7.

Carling GT, Fernandez DP, Rudd A, Pazmino E, Johnson WP. Trace element diel variations and particulate pulses in perimeter freshwater wetlands of Great Salt Lake, Utah. Chem Geol 2011;283:87-98.

Carling GT, Richards DC, Hoven H, Miller T, Fernandez DP, Rudd A, et al. Relationships of surface water, pore water, and sediment chemistry in wetlands adjacent to Great Salt Lake, Utah, and potential impacts on planet community health. Sci Total Environ 2013;443:798-811.

Chin YP, Traina SJ, Swank CR, Backhus D. Abundance and properties of dissolved organic matter in pore waters of a freshwater wetland. Limnol Oceanogr 1998;43:1287-96.

Compeau GC, Bartha R. Sulfate-reducing bacteria: principal methylators of mercury in anoxic estuarine sediment. Appl Environ Microbiol 1985;50:498-502.

Conover MR, Vest JL. Selenium and mercury concentrations in California gulls breeding on the Great Salt Lake, Utah, USA. Environ Toxicol Chem 2009a;28:324-9.

Conover MR, Vest JL. Concentrations of selenium and mercury in eared grebes (Podiceps nigricollis) from Utah's Great Salt Lake, USA. Environ Toxicol Chem 2009b;28:1319-23.

Diaz X, Johnson WP, Fernandez D, Naftz DL. Size and elemental distributions of nano- to micro-particulates in the geochemically-stratified Great Salt Lake. Appl Geochem 2009;24:1653-65.

Dong W, Liang L, Brooks S, Southworth G, Gu B. Roles of dissolved organic matter in the speciation of mercury and methylmercury in a contaminated ecosystem in Oak Ridge, Tennessee. Environ Chem 2010;7:94-102.

Gerbig CA, Kim CS, Stegemeier JP, Ryan JN, Aiken GR. Formation of nanocolloidal metacinnabar in mercury-DOM-sulfide systems. Environ Sci Technol 2011;45:9180-7.

Gondikas AP, Jang EK, Hsu-Kim H. Influence of amino acids cysteine and serine on aggregation kinetics of zinc and mercury sulfide colloids. Journ Colloid Interface Sci 2010;347:167-71.

Gorski PR, Armstrong DE, Hurley JP, Shafer MM. Speciation of aqueous methylmercury influences uptake by a freshwater alga (selenastrum capricornutum). Environ Toxicol Chem 2006;25:534-40.

Gorski PR, Armstrong DE, Hurley JP, Krabbenhoft DP. Influence of natural dissolved organic carbon on the bioavailability of mercury to a freshwater alga. Environ Pollution 2008;154:116-23.

Graham AM, Aiken GR, Gilmour CC. Dissolved organic matter enhances microbial mercury methylation under sulfidic conditions. Environ Sci Technol 2012;46:2715-23.

Gwynn JW. Great Salt Lake: chemical and physical variations of the brine and effects of the SPRR causeway, 1966-1996 in Gwynn, J.W., ed. Great Salt Lake: an overview of change. Utah Department of Natural Resources Special Publication 2002;87-106.

Hintelmann H, Evans RD. Application of stable isotopes in environmental tracer studies-Measurement of monomethylmercury (CH_3Hg^+) by isotope dilution ICP-MS and detection of species transformation. Fresenius J Anal Chem 1997;358:378-85.

Hintelmann H, Keppel-Jones K, Evans RD. Constants of mercury methylation and demethylation rates in sediments and comparison of tracer and ambient mercury availability. Environ Toxicol Chem 2000;19:2204-11.

Hintelmann H, Welbourn PM, Evans RD. Measurement of complexation of methylmercury(II) compounds by freshwater humic substances using equilibrium dialysis. Environ Sci Technol 1997;31:489-95.

Hsu-Kim H, Kucharzyk KH, Zhang T, Deshusses MA. Mechanisms regulating mercury bioavailability for methylating microorganisms in the aquatic environment: a critical review. Environ Sci Technol 2013;47:2441-56.

King JK, Kostka JE, Frischer ME, Saunders FM. Sulfate-reducing bacteria methylate mercury at variable rates in pure culture and in marine sediments. Appl Environ Microbiol 2000;66:2430-7.

Lambertsson L, Nilsson M. Organic material: the primary control on mercury methylation and ambient methyl mercury concentrations in estuarine sediments. Environ Sci Technol 2006;40:1822-9.

Loving BL, Waddell KM, Miller CW. Water and salt balance of Great Salt Lake, Utah, and simulation of water and salt movement through the causeway, 1963-98 in Gwynn, J.W., ed. Great Salt Lake: an overview of change. Utah Department of Natural Resources Special Publication 2002;143-65.

Marvin-DiPasquale M, Cox, MH. Legacy mercury in Alviso Slough, South San Francisco Bay, California: concentration, speciation and mobility. U.S. Geological Survey Open-File Report 2007-1240;2007.

Marvin-DiPasquale M, Lutz MA, Brigham ME, Krabbenhoft DP, Aiken GR, Orem WH, et al. Mercury cycling in stream ecosystems. 2. Benthic methylmercury production and bed sediment-pore water partitioning. Environ Sci Technol 2009;43:2726-32.

Marvin-DiPasquale M, Lutz MA, Krabbenhoft DP, Aiken GR, Orem WH, Hall BD, et al. Total mercury, methylmercury, methylmercury production potential, and ancillary streambed-sediment and pore-water data for selected streams in Oregon, Wisconsin, and Florida, 2003-04. U.S. Geological Survey: Reston, VA, Data Series 375;2008.

Mason RP, Heyes D, Sveinsdottir A. Methylmercury concentrations in fish from tidal waters of the Chesapeake Bay. Arch Environ Contam Toxicol 2006;51:425-37.

Miller T, Hoven H, Gray L, Rushforth S, Rushforth S, Cavitt J et al. Development of an assessment framework for impounded wetlands of Great Salt Lake. State of Utah: Department of Environmental Quality Report;2009.

Naftz D, Angeroth C, Kenney T, Waddell B, Darnall N, Silva S, et al. Anthropogenic influences on the input and biogeochemical cycling of nutrients and mercury in Great Salt Lake, Utah, USA. Appl Geochem 2008;23:1731-44.

Naftz DL, Cederberg JR, Krabbenhoft DP, Beisner KR, Whitehead J, Gardberg J. Diurnal trends in methylmercury concentration in a wetland adjacent to Great Salt Lake, Utah, USA. Chem Geol 2011;283:78-86.

Ranchou-Peyruse M, Monperrus M, Bridou R, Duran R, Amouroux D, Salvado JC et al. Overview of mercury methylation capacities among anaerobic bacteria including representatives of the sulphate-reducers: Implications for environmental studies. Geomicrobiol Journ 2009;1:1-8.

Scholl DJ, Ball RW. An evaluation of mercury concentrations in ducks from the Great Salt Lake, Utah for 2005 and 2006; Health Advisory Report. Utah Dept. of Health, Office of Epidemiology, Salt Lake City, UT, USA, 2006.

Sunderland EM, Gobas FPAC, Branfireun BA, Heyes A. Environmental controls on the speciation and distribution of mercury in coastal sediments. Marine Chem 2006;102:111-23.

USEPA Method 1630. Methylmercury in water by distillation, aqueous ethylation, purge and trap, and CVAFS; 2001a.

USEPA Method 1631 (Appendix). Appendix to method 1631: total mercury in tissue, sludge, sediment, and soil by acid digestion and BrCl oxidation; 2001b.

USEPA Method 1631, Revision E. Mercury in water by oxidation, purge and trap, and cold vapor atomic fluorescence spectrometry; 2002.

USEPA Method 1669. Sampling ambient water for trace metals at EPA water quality criteria levels; 1996.

USEPA Method 1684. Total, fixed, and volatile solids in water, solids, and biosolids; 2001c.

USEPA Method 200.8, Revision 5.4. Determination of trace elements in waters and wastes by inductively coupled plasma-mass spectrometry; 1994.

Windham-Myers L, Marvin-Dipasquale M, Krabbenhoft DP, Agee JL, Cox MH, Heredia-Middleton P, et al. Experimental removal of wetland emergent vegetation leads to decreased methylmercury production in surface sediment. Journ Geophysical Research: Biogeosci 2010;115:G00C05(14pp).

Zhang T, Kim B, Levard C, Reinsch BC, Lowry GV, Deshusses MA, et al. Methylation of mercury by bacteria exposed to dissolved, nanoparticulate, and microparticulate mercuric sulfides. Environ Sci Technol 2012;46:6950-8.

Zhong H, Wang W. Controls of dissolved organic matter and chloride on mercury uptake by a marine diatom. Environ Sci Technol 2009;43:8998-9003.